Developmental Biology 529 (2026) 66–80

Contents lists available at ScienceDirect

Developmental Biology

journal homepage: www.elsevier.com/locate/developmentalbiology

Original research article

WNT4 deficiency impacts heart, diaphragm, and palate development: Insights from human genetics, machine learning, and mouse models

Andrés Hernández-García [a], Bum Jun Kim [a], David Chitayat [b,c], Patrick Shannon [d], Stephanie Hedges [b], Maria Al Bandari [e], Maria J. Guillen Sacoto [f], Emily Anne Bates [g], Yunus H. Ozekin [h], Victor Faundes [i], Pamela N. Luna [a], Chad A. Shaw [a], Tara L. Rasmussen [j], Chih-Wei Hsu [j,k], Daryl A. Scott [a,l,*]

[a] Department of Molecular and Human Genetics, Baylor College of Medicine, Houston, TX, USA
[b] The Prenatal Diagnosis and Medical Genetics Program, Department of Obstetrics and Gynecology, Mount Sinai Hospital, University of Toronto, Toronto, Ontario, Canada
[c] Department of Pediatrics, Division of Clinical and Metabolic Genetics, The Hospital for Sick Children, University of Toronto, Toronto, Ontario, Canada
[d] Department of Pathology and Laboratory Medicine, Mount Sinai Hospital, University of Toronto, Toronto, Ontario, Canada
[e] Department of Clinical and Biochemical Genetics, National Genetics Center, Royal Hospital, Muscat, Sultanate of Oman
[f] GeneDx, LLC, Gaithersburg, MD, USA
[g] Department of Pediatrics, Section of Developmental Biology, University of Colorado Anschutz Medical Campus, Aurora, CO, USA
[h] Department of Medicine, University of Colorado Anschutz Medical Campus, Aurora, CO, USA
[i] Laboratorio de Genética y Enfermedades Metabólicas, Instituto de Nutrición y Tecnología de Los Alimentos, Universidad de Chile, Santiago, Chile
[j] Department of Integrative Physiology, Baylor College of Medicine, Houston, TX, USA
[k] Optical Imaging and Vital Microscopy Core, Baylor College of Medicine, Houston, TX, USA
[l] Baylor Genetics, Houston, TX, USA

ARTICLE INFO

Keywords:
WNT4
SERKAL syndrome
Ventricular septal defect
Congenital diaphragmatic hernia
Machine learning
Orofacial clefting
Gene prioritization
Developmental biology
Mouse phenotyping

ABSTRACT

WNT4 is a secreted protein that plays a critical role in the regulation of cell fate and embryogenesis. Biallelic variants in *WNT4* have been linked to SERKAL syndrome, an autosomal recessive disorder characterized by 46, XX sex reversal and dysgenesis of the kidneys, adrenals, and lungs. SERKAL syndrome has only been described in a single consanguineous kindred with four affected fetuses. Additional features seen in a subset of affected fetuses included ventricular septal defect (VSD), congenital diaphragmatic hernia (CDH), and orofacial clefting (OFC). To determine if these additional features were likely to be caused by WNT4 deficiency, we used machine learning to compare *WNT4* to genes known to cause VSD, CDH, and OFC. When compared to all RefSeq genes, WNT4's rank annotation scores for these congenital anomalies were 94%, 99%, and 98.5%, respectively, indicating a high level of similarity. We subsequently identified a second consanguineous family with SERKAL syndrome in which an affected fetus had CDH and an affected child had OFC. We then demonstrated that a subset of *Wnt4* null embryos have perimembranous VSDs, anterior and posterior sac CDH, and soft palate clefts. These findings suggest that WNT4 deficiency can cause VSD, CDH, and palatal anomalies in mice and humans with SERKAL syndrome. These studies also suggest that our machine learning approach can be used as a candidate gene prioritization tool, and that targeted mouse phenotyping can serve as a means of confirming the roles of candidate genes in mammalian development.

1. Introduction

Wingless-type MMTV integration site family, member 4 (*WNT4*), like other member of the WNT family of genes, encodes a secreted cysteine-rich lipoglycoprotein that acts as an extracellular signaling molecule through its interactions with frizzled (FZD) and other receptors (Nusse and Clevers, 2017). WNT4 is known to play a role in embryonic development, osteogenic differentiation, pancreatic β-cell maturation, decidual cell differentiation and decidualization, and neuronal and myofibroblast differentiation (Zhang et al., 2021).

* Corresponding author. R813 One Baylor Plaza, BCM225, Houston, TX, 77030, USA.
E-mail address: dscott@bcm.edu (D.A. Scott).

https://doi.org/10.1016/j.ydbio.2025.09.016
Received 19 September 2025; Accepted 20 September 2025
Available online 22 September 2025

Autosomal dominant *WNT4* missense variants have been shown to cause Mullerian aplasia and hyperandrogenism (MIM# 158330). (Biason-Lauber et al., 2004, 2007; Philibert et al., 2008) This disorder is characterized by aplasia/dysgenesis of Mullerian duct derivatives, virilization due to androgen excess, and in some cases unilateral renal agenesis (Biason-Lauber et al., 2004, 2007; Philibert et al., 2008). Functional studies suggest that at least a subset of these *WNT4* missense variants act in a dominant negative fashion (Biason-Lauber et al., 2007; Philibert et al., 2008). This is consistent with studies of female *Wnt4* null mice that have masculinized genitalia, absence of the Mullerian duct, atretic kidneys, reduced oocyte numbers, and failure of Leydig cell development in the ovary leading to ectopically activated testosterone biosynthesis (Stark et al., 1994; Vainio et al., 1999). These mice typically die perinatally.

In 2008, Mandel et al. described a consanguineous kindred in which a pair of siblings and their spouses had three pregnancies terminated between 19 and 24 weeks gestation due to ultrasound findings suggestive of renal agenesis (Mandel et al., 2008). Autopsies performed on these fetuses revealed largely overlapping features that included 46,XX sex reversal and dysgenesis of the kidneys, adrenals, and lungs. Mandel et al. proposed the acronym SERKAL to describe this syndrome (MIM# 611812). Other primary structural anomalies seen in a subset of these fetuses included ventricular septal defect (VSD) and pulmonary artery stenosis (n = 1), congenital diaphragmatic hernia (CDH, n = 1), and orofacial clefting (OFC, n = 2).

Based on WNT4's known role in renal and female development, Mandel et al. performed genotyping studies that found homozygosity by descent around *WNT4* on chromosome 1p36 (Biason-Lauber et al., 2004, 2007; Stark et al., 1994; Vainio et al., 1999). Subsequently, they identified a homozygous c.341C>T, p.(Ala114Val) [NM_030761.5] *WNT4* variant in one of the fetuses with SERKAL syndrome (Mandel et al., 2008). Parents and unaffected siblings in the kindred were found to be heterozygous. During Mandel et al.'s study, a fourth fetus was found to be homozygous for the c.341C>T variant and was terminated at 13 weeks gestation. Fetal amniocytes obtained from this pregnancy had markedly reduced *WNT4* mRNA levels, and OVCAR3 cells transfected with a *WNT4* vector carrying the c.341C>T variant had 2.8- to 3-fold lower *WNT4* transcript levels that cells transfected with a wild-type *WNT4* vector (Mandel et al., 2008). These findings suggested that the c.341C>T variant acts as a loss-of-function variant, and that SERKAL syndrome is caused by biallelic loss of WNT4 function.

Since Mandel et al.'s report, no additional individuals with SERKAL syndrome have been described. Since cardiac, diaphragmatic, and palatal anomalies have not been documented in *Wnt4* null mice, it remains unclear whether biallelic loss of WNT4 function can lead to VSD, CDH, and OFC in humans and/or mice.

Here, we use machine learning to demonstrate that *WNT4* is highly similar to genes known to cause VSD, CDH, and OFC. We subsequently describe a second family with SERKAL syndrome with biallelic variants in *WNT4*. This family included an affected fetus with CDH and an affected child with OFC. We then demonstrate that a subset *Wnt4* null embryos and mice have VSDs, anterior and posterior sac CDH, and soft palate clefts.

2. Materials and methods

2.1. Machine learning

We have previously used a machine learning algorithm to compare all RefSeq genes to a set of 31 training genes known to be associated with CDH and diaphragm development in humans and/or mice (Campbell et al., 2013; Callaway et al., 2018). Briefly, this tool integrates annotation data from various genome-scale knowledge sources to construct a pattern in genomic feature space based on a set of training genes associated with a specific phenotype and then ranks all RefSeq genes with respect to their similarity to that pattern using quantitative similarity metrics. Large-scale knowledge sources used by the algorithm including Gene Ontology (GO), Mouse Genome Informatics (MGI) phenotype annotation, the Protein Interaction Network Analysis platform (PINA), Kyoto Encyclopedia of Genes and Genomics (KEGG) molecular interaction network data, the GeneAtlas expression distribution, and transcription factor binding and epigenetic histone modification data from the NIH Roadmap Epigenetics Mapping Consortium (Blake et al., 2014; Ashburner et al., 2000; Cowley et al., 2012; Kanehisa et al., 2010). An omnibus phenotype-specific rank annotation score is then calculated which ranks the similarity of each RefSeq gene to the training gene set on a scale from 0% to 100%.

To generate rank annotation scores for ventricular septal defects (VSDs) and orofacial clefting (OFC), we identified review articles that contained lists of genes reported to cause these congenital anomalies and we searched the OMIM database to confirm these associations and to identify additional causative genes (Perrot and Rickert-Sperling, 2024; Chaithra et al., 2022; Cervantes-Salazar et al., 2024; Leslie and Marazita, 2013; Khan et al., 2020; Babai and Irving, 2023). Our final training gene sets consisted of 43 VSD genes (Supplemental Table S1) and 43 OFC genes (Supplemental Table S4) that were named in two or more of these sources. Fifty VSD genes and 58 OFC genes named in only one of these sources were designated as non-training VSD and OFC genes, respectively (Supplemental Tables S1 and S4).

As previously described, leave-one-out cross-validation studies were performed by iteratively excluding a single training gene and fitting the machine learning model using the remaining training genes (Callaway et al., 2018; Kunisetty et al., 2024). For each cross-validation instance, an evaluation of all RefSeq genes was performed, including the excluded training gene. The resulting scores were studentized, and the score of the excluded gene was recorded. The procedure was repeated so that each training gene received a cross-validated score. We then compared the studentized cross-validated scores of the training set genes to the scores of all other RefSeq genes derived from applying the machine learning model constructed using all training genes. Receiver operating characteristic (ROC) style curves were generated from this comparison in which the effectiveness of the procedure corresponds to the area under the curve and above the diagonal line which represents the result that would be generated by chance alone (Fig. 1A and C). An omnibus curve produced using fit data from all knowledge sources was positive, indicating that the algorithm could distinguish between the VSD- and OFC-associated genes in the training set and all other RefSeq genes better than random chance.

After validating our procedures, we generated VSD- and OFC-specific rank annotation scores for all RefSeq genes (Supplemental Tables S2 and S5). Our VSD and OFC training genes had median rank annotation scores of 98.9% and 98.7%, respectively (Fig. 1B and D). As a second means of validating our procedures, we then scored our non-training VSD and OFC genes with the assumption that although they did not meet criteria to be training genes, their respective sets would be enriched for bonafide VSD and OFC genes. The median rank annotation scores of the non-training VSD and OFC were 87.9% and 72.7%, respectively (Fig. 1B and D; Supplemental Tables S3 and S7). These median scores were well above the median score of all RefSeq genes (50 %) suggesting enrichment.

These scores also showed specificity to the VSD and OFC phenotypes, respectively as demonstrated by the lower median scores of genes that cause microphthalmia/anophthalmia/coloboma (MAC; 73.9% and 77.3%, respectively; $P < 0.0001$), epilepsy (72.1% and 76.9%, respectively; $P < 0.0001$), and 368 olfactory receptor genes (3.5% and 2.8%, respectively; $P < 0.0001$) (Supplemental Fig. S1 and S2; Supplemental Tables S4 and S8) (Campbell et al., 2013; Kunisetty et al., 2024).

2.2. WNT4 expression in the anterior palate

Published single-cell RNA sequencing data from the C57BL/6 E13.5 anterior palate was analyzed using the Seurat pipeline (Ozekin et al.,

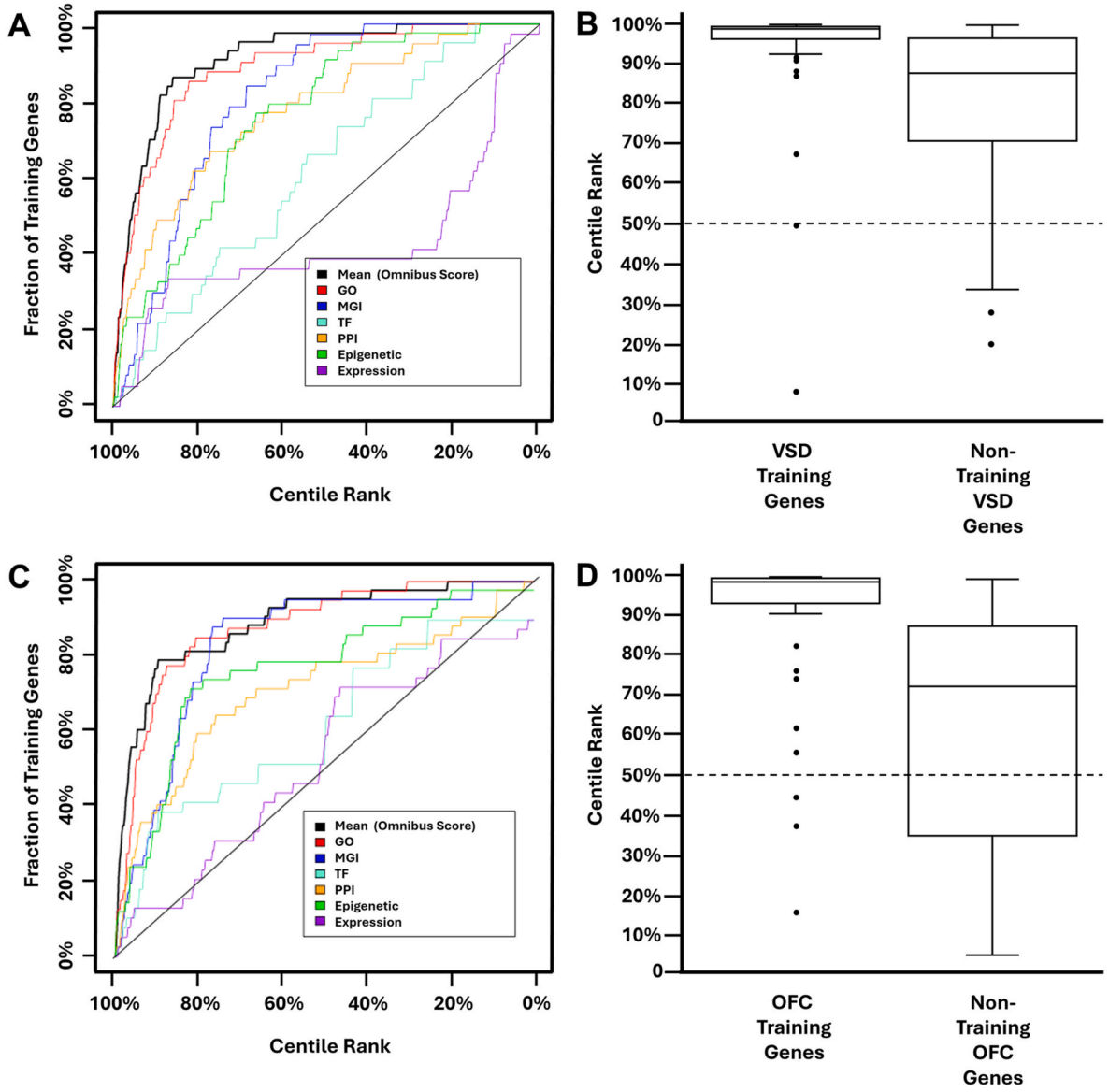

Fig. 1. Generating and validating VSD- and OFC-specific rank annotation scores for all RefSeq genes. A) A previously published machine learning algorithm was trained using 53 genes known to cause VSD in humans. Receiver operating characteristic (ROC) style curves were generated based on a leave-one-out validation study analysis performed for each knowledge source (colored lines). The area under the omnibus score (black curve) indicates the ability of the algorithm to identify genes in the training set more effectively than chance (diagonal black line). B) Box plots showing the algorithmically generated VSD-specific rank annotation scores for the VSD training genes (median score 98.9%) and 50 non-training VSD genes (median scores 87.9%) both of which demonstrate a shift towards higher scores compared to all RefSeq genes (dotted line). C) The same procedure was used to generate and validate OFC rank annotation scores based on a training gene set containing 43 human OFC genes. The resulting omnibus ROC style curve (black line) was positive. D) The median OFC-specific rank annotation scores for OFC training genes and 58 non-training OFC genes were 98.7% and 72.7% respectively. The scores of both groups demonstrated a shift towards higher scores compared to all RefSeq genes (dotted line in D). GO = Gene Ontology, MGI = Mouse Genome Informatics phenotype annotation, TF = transcription factor binding data from the NIH Roadmap Epigenetics Mapping Consortium, PPI = protein–protein integration networks.

2023; Stuart et al., 2019). Data was normalized using SingleCellTransform (SCT) and clustered at a resolution of 0.2 snn and integrated using the Seurat v4 integration method. Populations were identified based on marker gene expression (Ozekin et al., 2023).

2.3. Genetic and pathology evaluations

The genetic and pathology evaluations described in this manuscript were performed on a clinical basis. In accordance with international standards, parents provided consent for their publication.

Using genomic DNA from the proband fetus and parents, the exonic regions and flanking splice junctions of the genome were captured using the IDT xGen Exome Research Panel v1.0 (Integrated DNA Technologies, Coralville, IA). Massively parallel (NextGen) sequencing was done on an Illumina system with 150bp paired-end reads. Reads were aligned to human genome build GRCh37/UCSC hg19 and analyzed for sequence variants using a custom-developed analysis tool. Additional sequencing technology and variant interpretation protocols have been previously described (Retterer et al., 2016). The general assertion criteria for variant classification are publicly available on the GeneDx ClinVar submission page (http://www.ncbi.nlm.nih.gov/clinvar/submitters/26957/).

2.4. Multiple protein alignments

Multiple protein alignments were made using MAFFT version 7

(https://mafft.cbrc.jp/alignment/server/index.html). Aligned protein sequences correspond to human WNT4 (NM_030761.5), rat WNT4 (NM_053402.2), mouse WNT4 (NM_009523.2), zebrafish wnt4 (NM_001040387.1), *Xenopus* wnt4.L (NM_001087728.1), *Drosophila* Wnt4 (NM_057624.4), and *C. elegans* cwn-1 (predicted homolog, NM_061267.5) (Katoh et al., 2002; Wang et al., 2017).

2.5. Mouse models

Mice bearing the *Wnt4* GCE knock-in/knock-out allele (*Wnt4*^{GCE}, Jackson Laboratory, strain # 032489) have been previously described (Kobayashi et al., 2008). This allele abolishes *Wnt4* gene function and expresses a EGFP and creERT2 (eGFPCreERT2) fusion protein from the *Wnt4* promoter/enhancer elements. In this manuscript, we refer to embryos and mice that are heterozygous or homozygous for this allele as being *Wnt4*$^{+/-}$ and *Wnt4*$^{-/-}$ (*Wnt4* null), respectively.

All mice in our study were maintained on a C57BL/6 background. All experiments using mouse models were conducted in accordance with the recommendations in the Guide for the Care and Use of Laboratory Animals of the National Institutes of Health (NIH). The associated protocols were approved by the Institutional Animal Care and Use Committee of Baylor College of Medicine (Animal Welfare Assurance #A3832-01).

2.6. Histology

For standard histology, embryos were fixed in buffered Formalde-Fresh Solution (Fisher) or 4 % buffered paraformaldehyde (PFA). After fixation, the specimens were washed in PBS, dehydrated in ethanol, embedded in paraffin, and sectioned at 10 μm. Series of sections were then stained with hematoxylin and eosin (H&E).

2.7. Protein modeling

The predicted WNT4 structure was downloaded from the Alphafold database (entry AF-P56705-F1) and the crystal structure of *Xenopus* wnt8 (Xwnt8) in complex with the cysteine-rich domain (CRD) of mouse FZ8 (Fz8-CRD) was downloaded from the RCSB Protein Data Bank (pdb_00008ctg). Protein modeling was performed using UCSF Chimera 1.10 and ChimeraX v1.9 software (Pettersen et al., 2004; Meng et al., 2023).

2.8. Micro-CT analyses

Specimen were processed as previously described (Hsu et al., 2019). Briefly, mouse embryos and newborn pups were obtained and fixed in 4% PFA for at least 1 week. They were then stabilized using a modified Stability buffer (mStability) which includes 4% acrylamide (BIO-RAD, cat. no. 1610140), 0.25% w/v VA044 (Wako Chemical, cat. no. 017–19362), 0.05% w/v saponin (MilliporeSigma, cat. no. 84510), and 0.1% sodium azide. Samples were allowed to come to equilibrium in the hydrogel solution for at least 7 days. The samples in hydrogel were subjected to a thermo-induced crosslinking reaction for 3 h at −90 kPa at 37 °C. After the crosslinking, the remaining hydrogel solution was removed, and specimens were washed four times in 1X PBS. Samples were then immersed in 0.1N iodine and incubated with gentle agitation for at least 10 days before mounting in agarose and imaging on a Bruker Skyscan 1272 scanner (Bruker, Kontich, Belgium) using a 0.5 mm aluminum filter. The resulting metadata was processed using NRecon software (Bruker, Kontich, Belgium) and converted to a Nrrd format using Harwell Automated Recon Processor (HARP), an open-source, cross-platform application developed in Python (Brown et al., 2016). The 3D volumes were analyzed, and optical sections were captured using 3D Slicer (Fedorov et al., 2012).

2.9. Statistical analyses

Phenotype frequency comparisons between control and *Wnt4*$^{-/-}$ embryos and newborn pups were made using online 2 X 2 contingency tables from GraphPad (https://www.graphpad.com/quickcalcs/contingency1/) to generate P values using a two-tailed Fisher's exact test. Wilson score 95% confidence intervals (95% CI) were generated using the Proportion Confidence Interval Calculator from Statistic Kingdom (https://www.statskingdom.com/proportion-confidence-interval-calculator.html). Box plots were draw with the aid of the Statistics Calculator: Box Plot tool from Alcula (https://www.alcula.com/calculators/statistics/box-plot/).

3. Results

3.1. WNT4 is highly similar to genes known to cause VSDs, CDH, and OFC

We have previously used machine learning to prioritize candidate genes for various congenital anomalies, including CDH, for further evaluation. (Callaway et al., 2018)' (Cowley et al., 2012)' (Brown et al., 2016; Fedorov et al., 2012; Russell et al., 2012) Our approach is based on the hypothesis that unidentified genes that cause a particular phenotype will be more similar to genes already known to cause that phenotype than genes which do not. In this approach, we use a published machine learning algorithm to generate a phenotype-specific rank annotation score for each RefSeq gene (Campbell et al., 2013). We used a similar approach to generate VSD- and OFC-specific rank annotation scores for all RefSeq genes (Supplemental Tables S2 and S4).

WNT4 received CDH-, VSD- and OFC-specific rank annotation scores of 99%, 94%, and 98.5%, respectively. This high level of similarity to genes known to cause these congenital anomalies suggested that *WNT4* was an excellent VSD, CDH, and OFC candidate gene worthy of further evaluation (Callaway et al., 2018). This conclusion was supported by expression studies in which WNT4 has been shown to be expressed in the endocardium of the atrioventricular (AV) canal at E10.5 and E12.5, the developing mouse diaphragm at E11.5, E12.5, and E16.5, and the epithelial cells of the anterior palate at E13.5 (Supplemental Fig. S3) (Ozekin et al., 2023; Russell et al., 2012; Wang et al., 2013; Alfieri et al., 2010).

3.2. A second consanguineous family with SERKAL syndrome

SERKAL syndrome was originally described by Mandel et al. in a single consanguineous kindred in 2008 (Fig. 2A). (Mandel et al., 2008) Since that time, no other individuals or families with SERKAL syndrome has been reported. We identified a consanguineous Afghan family with SERKAL syndrome (Fig. 2B). The 27-year-old G3P1SA1L1 mother and 30-year-old father were healthy second cousins. The family history was non-contributory. Their first pregnancy was complicated by oligohydramnios and the male fetus was found to have unilateral renal agenesis on ultrasound. The couple decided to continue the pregnancy despite concerns for poor prognosis. Their son was born at term but died shortly after delivery. On external examination, he was noted to have a cleft lip. An autopsy was declined. Their second pregnancy resulted in a miscarriage at 8 weeks gestation.

The couple's third pregnancy was documented to be free from bleeds, fever, infections, rashes, hypertension, diabetes, or exposure to teratogens. However, an ultrasound examination at 21 1/7 weeks gestation showed anhydramnios, a two-vessel cord, dolichocephaly, non-visualization of the stomach and kidneys, and "lying-down adrenals" suggestive of renal agenesis. The bladder was present. The abdominal circumference was at the 5th centile. The couple was counseled and decided to interrupt the pregnancy. They agreed to a fetal autopsy.

The autopsy of the proband fetus showed abnormal facies with

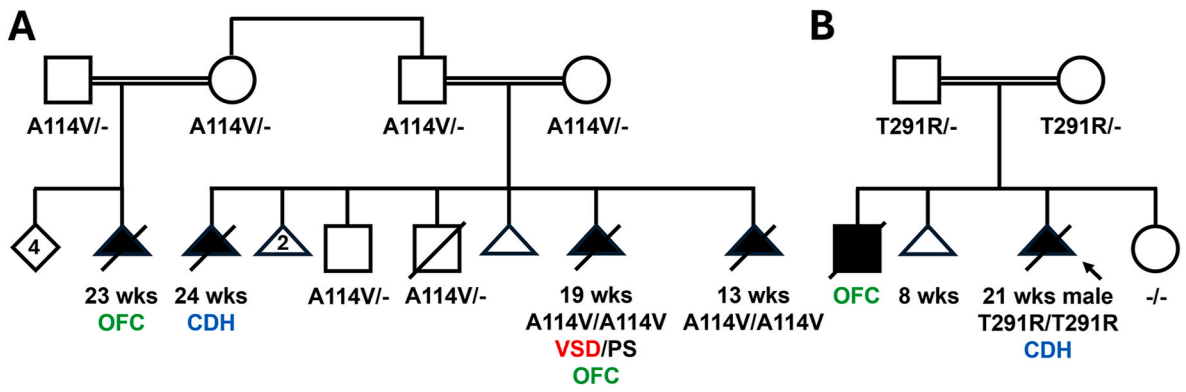

Fig. 2. Consanguineous families with SERKAL syndrome. A) A simplified pedigree of the consanguineous kindred previously reported by Mandel et al. in which homozygous *WNT4* c.341C>T, p.(Ala114Val) [NM_030761.5] missense variants (A114V) segregated with SERKAL syndrome phenotypes. A subset of affected fetuses had ventricular septal defect/pulmonary stenosis (VSD/PS), orofacial clefting (OFC), and/or congenital diaphragmatic hernia (CDH) as indicated. B) Pedigree of the second consanguineous family described in this manuscript in which homozygous *WNT4* c.872C>G, p.(Thr291Arg) [NM_030761.5] missense variants (T291R) segregated with SERKAL syndrome phenotypes. An affected fetus had CDH and an affected male child had OFC as indicated.

findings consistent with Potter sequence including low set, posteriorly rotated ears, flattened nose, and downturned corners of mouth. There was redundant skin and multiple joint contractures with axillary, antecubital, and inguinal pterygia. The hips and knees were fixed in extension position. The thorax was tubular and narrow, and the left umbilical artery was absent. Internal abnormalities included bilateral agenesis of the diaphragm, pulmonary hypoplasia, bilateral renal hypoplasia with cystic dysplasia, agenesis of the right adrenal, and marked hypoplasia of the left adrenal (Fig. 3A and B). Histological analyses of the left adrenal revealed partial cystic change superiorly with attached small tubular structures resembling Wolffian remnants (Fig. 3C and D).

A chromosomal microarray analysis showed a normal male pattern. Clinical trio exome sequencing revealed a biparentally inherited homozygous c.872C>G, p.(Thr291Arg) [NM_030761.5] variant of uncertain significance in *WNT4*. This variant was highly conserved (Fig. 4A), was predicted to be "Disease Causing" by MutationTaster, and had a CADD score of 27.5 and a REVEL score of 0.809 (Schwarz et al., 2014; Schubach et al., 2024; Ioannidis et al., 2016). A diagnosis of SERKAL syndrome was made with the deceased sibling also being thought to have SERKAL syndrome.

This couple's 4th pregnancy ended in the birth of a normal female (Fig. 2B). Postnatal cord blood testing revealed that she was not a carrier of the c.872C>G *WNT4* variant.

3.3. *In silico protein modeling of SERKAL-causing WNT4 variants*

In silico protein modeling indicates that alanine 114 (A114), which is substituted by valine in the original SERKAL kindred described by Mandel et al., is located in an alpha coil (Fig. 4B). The threonine 291 (T291), which is substituted by arginine in the second SERKAL family that we describe, is located at the junction between the "index finger" and "hand" regions of human WNT4 (Fig. 4B and C). (Janda et al., 2012) The "index finger" region interacts with the cysteine-rich domains (CRD) of Frizzled receptors based on structural superimposition on the structure of *Xenopus* Wnt8 (XWnt8) in complex with the mouse Frizzled-8 CRD (Fz8-CRD) (Fig. 4C). (Janda et al., 2012)

The c.341C>T, p.(Ala114Val) variant is thought to cause loss of WNT4 function, at least in part, due to its effect on mRNA stability (Mandel et al., 2008). Protein modeling suggests that the replacement of the non-polar, aliphatic alanine 114 (A114) by a non-polar, branched-chain valine is not predicted to cause the loss of any hydrogen bonds but is predicted to lead to five steric hinderances (Fig. 4D–F). In contrast, the substitution of the polar T291 with a positively charged arginine is predicted to cause the loss of three hydrogen bonds and lead to 19 steric hinderances (Fig. 4G, H). These changes may lead to loss of WNT4 function through their adverse effects on protein folding, structure, and/or receptor binding (Stollar and Smith, 2020).

3.4. *A subset of Wnt4 null embryos have VSDs*

Despite the fact that WNT4 has been shown to function in the development of the endocardial cushions of the AV canal, cardiovascular malformations have not been documented in *Wnt4* null mice (Stark et al., 1994; Vainio et al., 1999; Wang et al., 2013; Hong et al., 2021; Hernandez-Garcia et al., 2023). To determine if WNT4 deficiency can cause cardiac defects in mice, we crossed $Wnt4^{+/-}$ mice and harvested the resulting embryos at E15.5-E16.5. At this timepoint, 100% (16/16) wild-type embryos had intact ventricular septa (Fig. 5A–A'). In contrast, perimembranous VSDs were identified in 33% (3/9; $P = 0.037$; 95% CI = 0.12 to 0.65) of $Wnt4^{-/-}$ embryos (Fig. 5B–B', C, C').

3.5. *A subset of Wnt4 null embryos have non-muscularized regions of their anterior and posterior diaphragm*

To determine if WNT4 deficiency can cause CDH in mice, we crossed $Wnt4^{+/-}$ mice and harvested embryos at E17.5-E18.0. After fixation, their diaphragms were microdissected and analyzed. At this time point, 100% (11/11) of wild type embryos had complete muscularization of their anterior diaphragms with only a small, amuscular separation between the right and left muscularized regions. The diaphragm of the wild-type embryo with the most prominent anterior separation is shown in Fig. 6A–C. The posterior muscularization of the diaphragm was also complete in 100% (11/11) of wild-type embryos (Fig. 6A–C).

In contrast to wild-type control embryos, 100% (7/7; 95% CI = 0.60 to 1) $Wnt4^{-/-}$ embryos had large gaps between the muscularized regions of their right and left anterior diaphragm (Fig. 6D and E; $P < 0.0001$). Absence and/or thinning of the musculature over the posterior regions of the diaphragm was identified in 57% (4/7; 95% CI = 0.25 to 0.84) of these embryos with one having a right-sided defect, one having a left-sided defect, and two having bilateral defects (Fig. 6D–F; $P = 0.0114$). These amuscular/hypomuscular regions appeared to be redundant and/or to form a pocket, suggesting that they were likely to represent the membranous coverings of a sac hernias whose contents had been removed by microdissection.

3.6. *Micro-CT analyses identify VSD, CDH, and soft palate clefts in $Wnt4^{-/-}$ embryos and newborn pups*

To confirm that WNT4 deficiency causes VSD, and that the amuscular/hypomuscular regions of the diaphragm seen in E17.5-E18.0

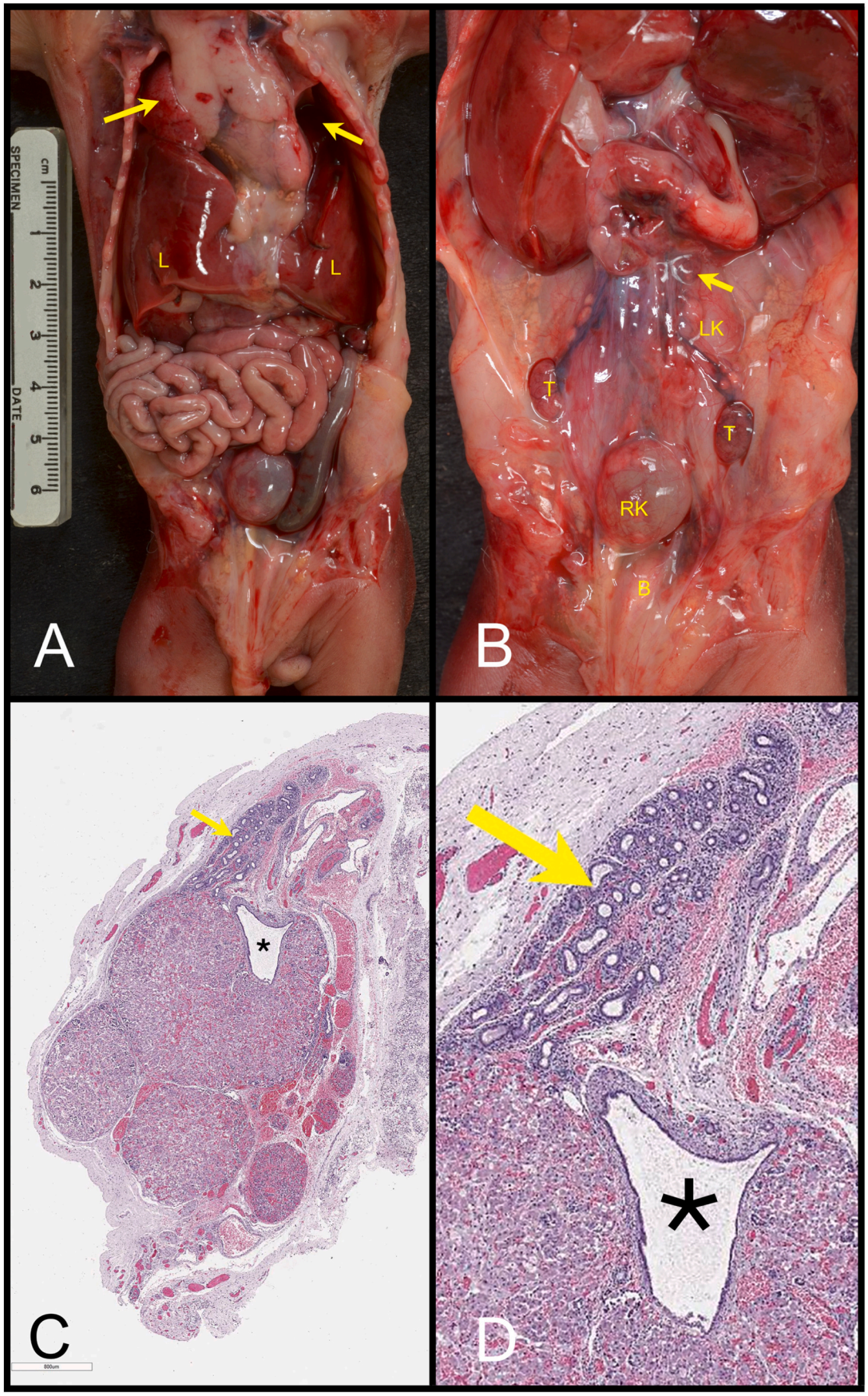

(caption on next page)

Fig. 3. Autopsy findings in a fetus with SERKAL syndrome. A) Fetal autopsy photo with the chest and abdominal walls reflected, demonstrate a narrow, elongated thorax with minute lungs compressed into the apex of the thorax (yellow arrows). The liver (L) has completely ascended into the ribcage and there is no diaphragm separating it from the lungs. B) Fetal autopsy photo of the retroperitoneum with bowel, pancreas, and spleen removed. The right kidney (RK) is a cystic structure at the edge of the pelvis with small nodules of renal tissue in the walls. The left kidney (LK) is a minute nodule of renal tissue. The bladder (B) is tubular, and the testes (T) are histologically normal and appropriately undescended. The right adrenal is absent, and the left is a small nodule (arrow) high in the retroperitoneal cavity. C) Whole mounted left adrenal with partial cystic change (superior, asterisk) attached to small tubules resembling Wolffian remnants (arrow). D) Magnified view of the boxed region of panel C with partial cystic changes (asterisk) and Wolffian remnants (arrow) marked.

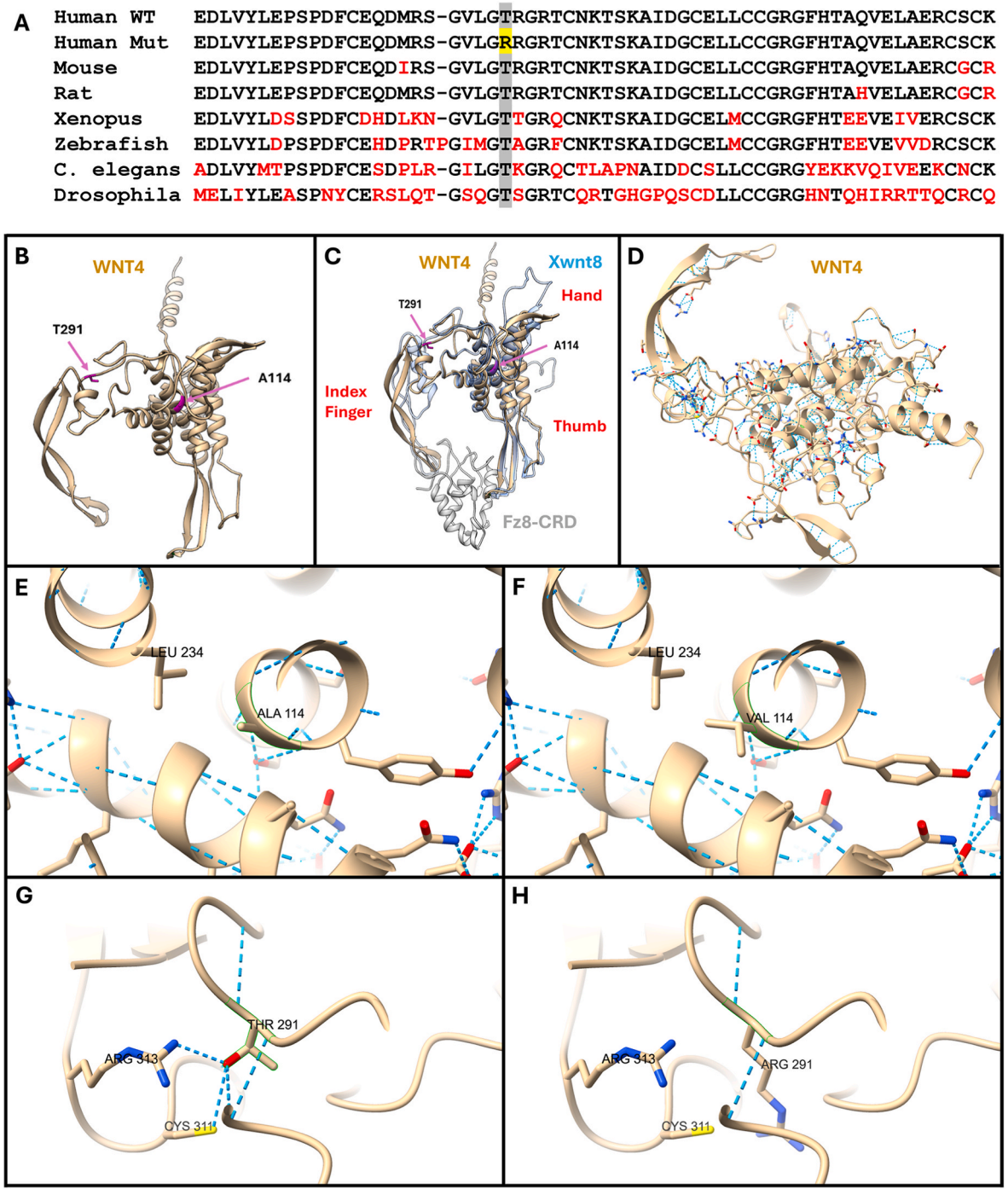

Fig. 4. SERKAL-causing WNT4 variants. A) Multiple protein alignments demonstrate that the threonine residue at position 291 (T291) in human WNT4 is highly conserved (gray background). The arginine residue at position 291 is marked with a yellow background, and non-conserved residues are shown in red. B) Predicted structure of WNT4 with the positions of alanine 114 (A114) and T291 shown in magenta. C) Superimposition of WNT4 (tan) on the crystalline structure of *Xenopus* wnt8 (Xwnt8; light blue) in complex with the cysteine-rich domain (CRD) of mouse FZ8 (Fz8-CRD; silver). T291 is located at the junction between the "index finger" region, which interacts with the CRDs of Frizzled receptors, and the "hand" region of WNT4. D) Predicted structure of WNT4 with hydrogen bonds shown as dashed blue lines. E-F) The substitution of valine for alanine at position 114 is not predicted to cause the loss of any hydrogen bonds but is predicted to lead to five steric hinderances. G-H) The substitution of arginine for threonine at position 291 is predicted to cause the loss of three hydrogen bonds and lead to 19 steric hinderances.

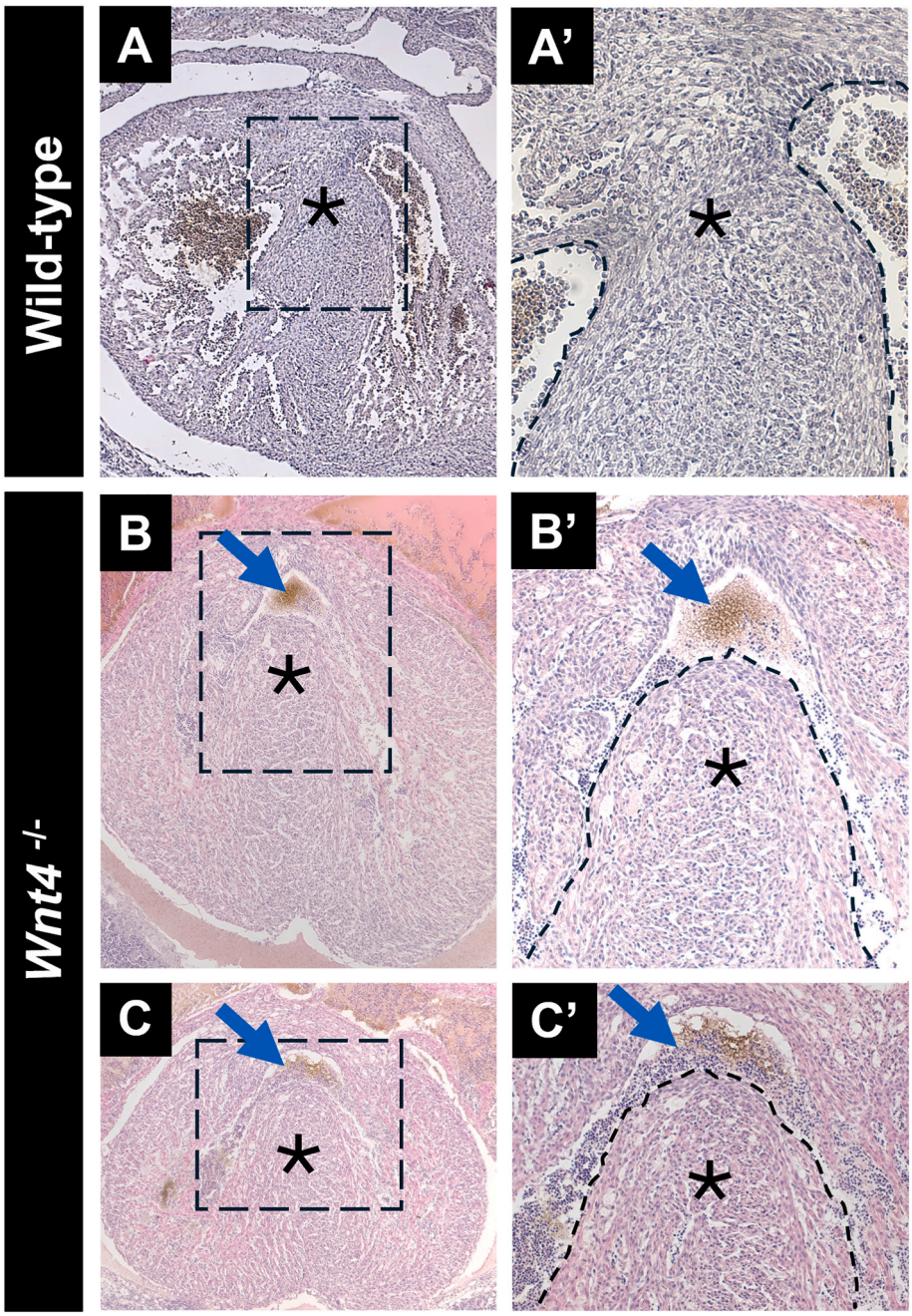

Fig. 5. WNT4 deficiency causes VSDs in mice. A) By E15.5, the right and left ventricles are separated by the interventricular septum (*) in wild-type C57BL/6 mice. A′) A magnified image of the area marked by the black rectangle in panel A. In this view, the endocardium is marked with dashed lines. B, C) In contrast, 33% (3/9) *Wnt4*$^{-/-}$ embryos had perimembranous VSDs (blue arrows) that interrupted their ventricular septa (*). B′, C′) Magnified images of the areas marked by the black rectangle in corresponding panels. In these panels, the endocardium is marked with dashed lines, and the ventricular septal defect is marked by a blue arrow. Blood cells are seen between the endocardial layers.

Wnt4$^{-/-}$ embryos represented membranes covering sac hernias, we crossed *Wnt4*$^{+/-}$ mice and harvested a litter of E17.0 embryos (one wild-type, two *Wnt4*$^{+/-}$, and three *Wnt4*$^{-/-}$ embryos), two wild-type newborn pups, and six *Wnt4*$^{-/-}$ newborn pups. After fixation, these embryos and newborn pups were submitted for micro-CT analysis and phenotyped in a blinded fashion (Table 1). As expected, none of the wild-type or *Wnt4*$^{+/-}$ embryos and newborn pups had abnormalities noted with the exception of one E17.0 *Wnt4*$^{+/-}$ embryo that had a small jaw. In contrast, small or absent kidneys were seen in 89% (8/9) of *Wnt4*$^{-/-}$ embryos and newborn pups consistent with previous reports (Kobayashi et al., 2008). VSDs were also seen in 56% (5/9) of *Wnt4*$^{-/-}$ embryos and newborn pups, confirming the results of our histological analyses (Fig. 7).

The micro-CT analyses of the wild-type embryos and newborn pups revealed normal anterior muscularization with only a thin strip of non-muscularized diaphragm between the right and left muscularized regions, normal muscularization in the posterior diaphragm, and no evidence of liver herniation (Fig. 8A and B). In contrast to wild-type controls, 56% (5/9) of the *Wnt4*$^{-/-}$ embryos and newborn pups had large non-muscularized regions of the anterior diaphragm with some having underlying outgrowths of liver consistent with sac CDH (Fig. 8C and D).

Posterior sac hernias with liver herniation were not documented in E17.0 *Wnt4*$^{-/-}$ embryos but were seen in 50% (3/6) of the *Wnt4*$^{-/-}$

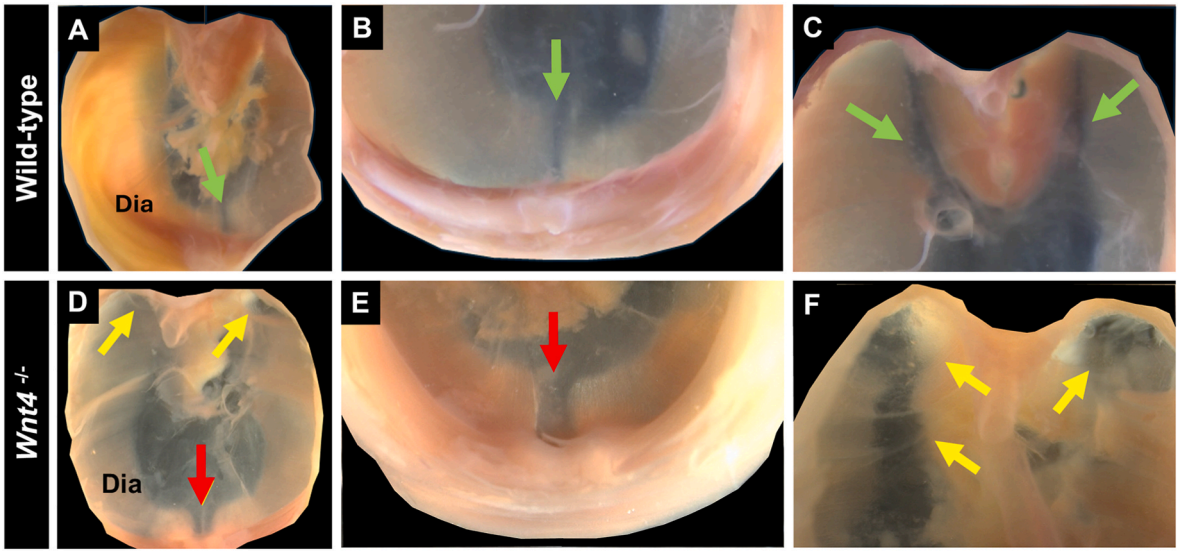

Fig. 6. WNT deficiency leads to abnormal muscularization of the diaphragm. A-C) At E17.5-E18, wild type C57BL/6 mice have fully muscularized diaphragms with only a small region of non-muscularized diaphragm located between the anterior right and left muscularized regions (green arrows in A and B). Similar regions of non-muscularized diaphragm are seen posteriorly (green arrows in C). D) The diaphragm of a *Wnt4*$^{-/-}$ E17.5-E18 embryo demonstrates a large gap between the muscularized regions of the anterior diaphragm (red arrow) and large amuscular/hypomuscular regions of the posterior diaphragm (yellow arrows). E-F) Anterior and posterior views of the diaphragm of a second *Wnt4*$^{-/-}$ E17.5-E18 embryo show a large gap between the muscularized regions of the anterior diaphragm (red arrow in E), and large amuscular/hypo-muscular regions of the posterior diaphragm (yellow arrows in F).

Table 1
Blinded micro-CT analyses.

Age	Genotype	Renal	VSD	Anterior CDH	Posterior CDH	Soft Palate Cleft
E17.0	Wild-type	–	–	–	–	–
E17.0	*Wnt4*$^{+/-}$ (het)	–	–	–	–	–
E17.0	*Wnt4*$^{+/-}$ (het)	–	–	–	–	–
E17.0	*Wnt4*$^{-/-}$ (null)	B small	+	+	–	+
E17.0	*Wnt4*$^{-/-}$ (null)	B small	–	+	–	+
E17.0	*Wnt4*$^{-/-}$ (null)	R absent; L small	+	+	–	+
Newborn pup	Wild-type	–	–	–	–	–
Newborn pup	Wild-type	–	–	–	–	–
Newborn pup	*Wnt4*$^{-/-}$ (null)	B small	+	+	B	+
Newborn pup	*Wnt4*$^{-/-}$ (null)	B small	+	+	B	+
Newborn pup	*Wnt4*$^{-/-}$ (null)	–	–	–	R	–
Newborn pup	*Wnt4*$^{-/-}$ (null)	B small	–	–	–	+
Newborn pup	*Wnt4*$^{-/-}$ (null)	B absent	–	–	–	+
Newborn pup	*Wnt4*$^{-/-}$ (null)	B small	+	–	–	+
	Percent affected of nulls animals	89 % (8/9)	56 % (5/9)	56 % (5/9)	33 % (3/9)	89 % (8/9)

* Small jaw. - = absent, + = present, B = bilateral, CHD = congenital diaphragmatic hernia, L = left, R = right, VSD = ventricular septal defect.

newborns with one pup having a right-sided sac CDH and two newborn pups having bilateral sac CDH (Fig. 8E–H).

Gross dissections of 5 *Wnt4*$^{-/-}$ E18.0 embryos and 6 *Wnt4*$^{-/-}$ newborn pups did not reveal evidence of cleft lip or cleft palate (data not shown). Micro-CT analyses also showed normal palates in wild-type and *Wnt4*$^{+/-}$ E17.0 embryos and newborn pups. In contrast, micro-CT analyses demonstrated that 89% (8/9; P = 0.0030; 95% CI 0.57 to 0.98) of *Wnt4*$^{-/-}$ E17.0 embryos and newborn pups had soft palate clefts (Table 1, Fig. 9).

4. Discussion

4.1. Prioritizing candidate genes using machine learning

Differentiating between genes that contribute to the development of cardiac, diaphragm, and palatal defects, and those that do not, often involves time consuming and expensive studies involving large cohorts or animal models (Qiao et al., 2021; Beck et al., 2013; Jordan et al., 2018). Hence, prioritizing candidate genes for further study has become increasingly important to gene discovery efforts. We have previously used our machine learning approach to prioritize positional candidate genes for CDH from the Wolf-Hirschhorn syndrome (WHS) critical region for CDH on chromosome 4p16.3, and as an aid to identifying low-penetrance genes for CDH from sequence and copy number variant data (Callaway et al., 2018; Scott et al., 2021; Hardcastle et al., 2022).

Here, we generated VSD- and OFC-specific rank annotation scores for these phenotypes (Supplemental Tables S3 and S6, respectively). *WNT4*'s high VSD-, CDH-, and OFC-specific rank annotation scores of 94%, 99%, and 98.5%, respectively, and *Wnt4* expression in the developing heart, diaphragm, and palate, led us to prioritize this gene for further study (Callaway et al., 2018).

We have used similarly generated rank annotation scores as a means

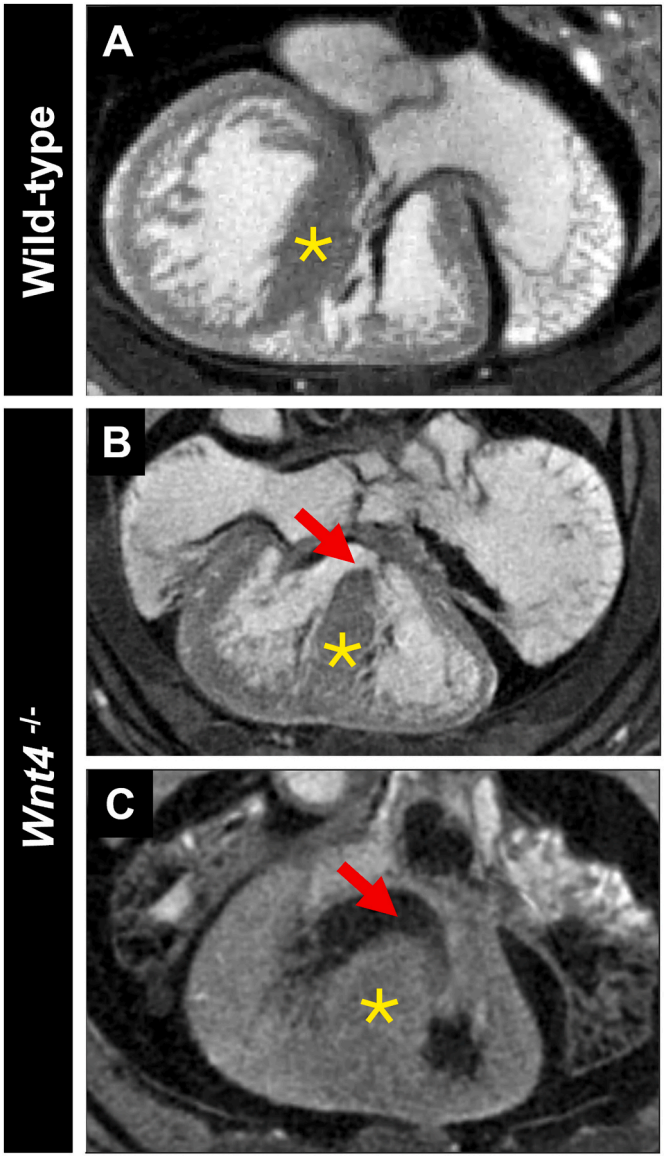

Fig. 7. Micro-CT analyses confirm that *Wnt4*$^{-/-}$ embryos have ventricular septal defects. A-C) Micro-CT images confirm the presence of interrupted ventricular septa (*) and perimembranous VSDs (red arrows) in *Wnt4*$^{-/-}$ embryos at E17.0.

of prioritizing candidate genes for other congenital anomalies including esophageal atresia/tracheoesophageal fistula, anorectal malformations, total anomalous pulmonary venous return, and microphthalmia/anophthalmia/coloboma (Kunisetty et al., 2024; Belanger Deloge et al., 2023; Huth et al., 2023; Sy et al., 2022). Although we have shown that our machine learning approach can be an aid to gene discovery efforts, it cannot be used in isolation as a means of defining candidate genes since, by definition, 10% of all genes in the genome have rank annotation scores of ≥ 90%. Its proper application is in the prioritization of genes for which there is already some evidence suggesting causality.

4.2. SERKAL syndrome variants

The *WNT4* variant seen in the original SERKAL kindred described by Mandel et al. (c.341C>T, p.(Ala114Val) [NM_030761.5]) was shown to be a loss of function variant (Mandel et al., 2008). Since all of the heterozygous parents in this kindred were asymptomatic and fertile, we can assume that both males and females can lose all or most of the WNT4 function from a single allele, without serious medical consequences. This is in keeping with WNT4's probability of loss of function intolerance (pLI score) of 0.05 and loss-of-function observed/expected upper bound fraction (LOEUF score) of 0.69, and the fact that heterozygous *Wnt4*$^{+/-}$ mice are also viable and fertile (Kobayashi et al., 2008; Karczewski et al., 2020). This recessive inheritance pattern, the overlapping phenotypes seen in the SERKAL syndrome family we describe, and protein modeling (Fig. 4) suggest that the c.872C>G, p.(Thr291Arg) [NM_030761.5] allele is also likely to be loss-of-function.

The phenotypes seen in SERKAL syndrome are more extensive than those seen in Mullerian aplasia and hyperandrogenism syndrome which are limited to aplasia/dysgenesis of Mullerian duct derivatives, virilization due to androgen excess, and in some cases unilateral renal agenesis (Biason-Lauber et al., 2004, 2007; Philibert et al., 2008). Mullerian aplasia and hyperandrogenism syndrome is caused by mono-allelic missense variants in *WNT4* that have been shown to have a dominant negative effect. This suggests that the biallelic *WNT4* variants that cause SERKAL syndrome are likely to be associated with a greater decrease in WNT4 function than the heterozygous dominant negative *WNT4* variants that cause Mullerian aplasia and hyperandrogenism.

4.3. Expansion of the SERKAL syndrome phenotype to include CDH and OFC

With the identification of the second family with SERKAL syndrome, the human evidence that loss of WNT4 function causes CDH and OFC are significantly strengthened. Affected individuals from both families have the same type of CDH, diaphragm agenesis (n = 2), and the same type of OFC, cleft lip ± cleft palate (CL ± P; n = 3). Taking a conservative approach in which we assume the incidence of the incidence for CDH is 1:2500 and the incidence of CL ± P is 1:500 in the general population, the rate at which these defects have been reported in individuals with SERKAL syndrome—30% (2/6) and 50% (3/6), respectively—are significantly higher that what would be expected by chance ($P < 0.0001$) (olitis et al., 2021; Mossey and Modell, 2012).

4.4. WNT4 loss of function as a cause of ventricular septal defects

Only one individual with SERKAL syndrome has been shown to have VSD, which is insufficient to demonstrate that loss of WNT4 function is sufficient to cause this type of congenital heart defect. However, a molecular mechanism by which loss of WNT4 function could lead to the development of VSD has also been outlined previously.

The development of the AV cushions, which will ultimately give rise to the AV septum and its associated valves, requires multiple steps including cell commitment, deposition of the cardiac jelly, delamination of the endocardium, endocardial to mesenchymal transition (EndMT), and mesenchymal cell proliferation (Kaneko et al., 2008; Rivera-Feliciano and Tab lesin and 2006; Combs and Yutzey, 2009; Eisenberg and Markwald, 1995; Lin et al., 2012). Crosstalk between the endocardium and myocardium of the AV canal is essential for EndMT, the process by which cells exit the endothelium and transform into mesenchymal cells that accumulate in the cardiac jelly (Kovacic et al., 2019). *Wnt4* is expressed in the endocardium of the developing AV canal (Wang et al., 2013; Alfieri et al., 2010). Its expression has been shown to be regulated by Jagged1-Notch1 signaling and SOX7 (Wang et al., 2013; Hong et al., 2021; Hernandez-Garcia et al., 2023). After secretion from the endocardium, WNT4 acts as a paracrine factor and upregulates *Bmp2* expression in the adjacent AV canal myocardium (Wang et al., 2013). BMP2, in turn, is secreted from the myocardium and acts as a paracrine factor to increase both EndMT and mesenchymal cell proliferation in the developing endocardial cushion (Ma et al., 2005).

Hernandez et al. provided in-vivo evidence in support of this model by demonstrating that *Sox7* and *Wnt4* interact genetically in the development of VSDs with *Sox7*$^{+/-}$;*Wnt4*$^{+/-}$ double heterozygous embryos having muscular and perimembranous VSD not seen in their *Sox7*$^{+/-}$

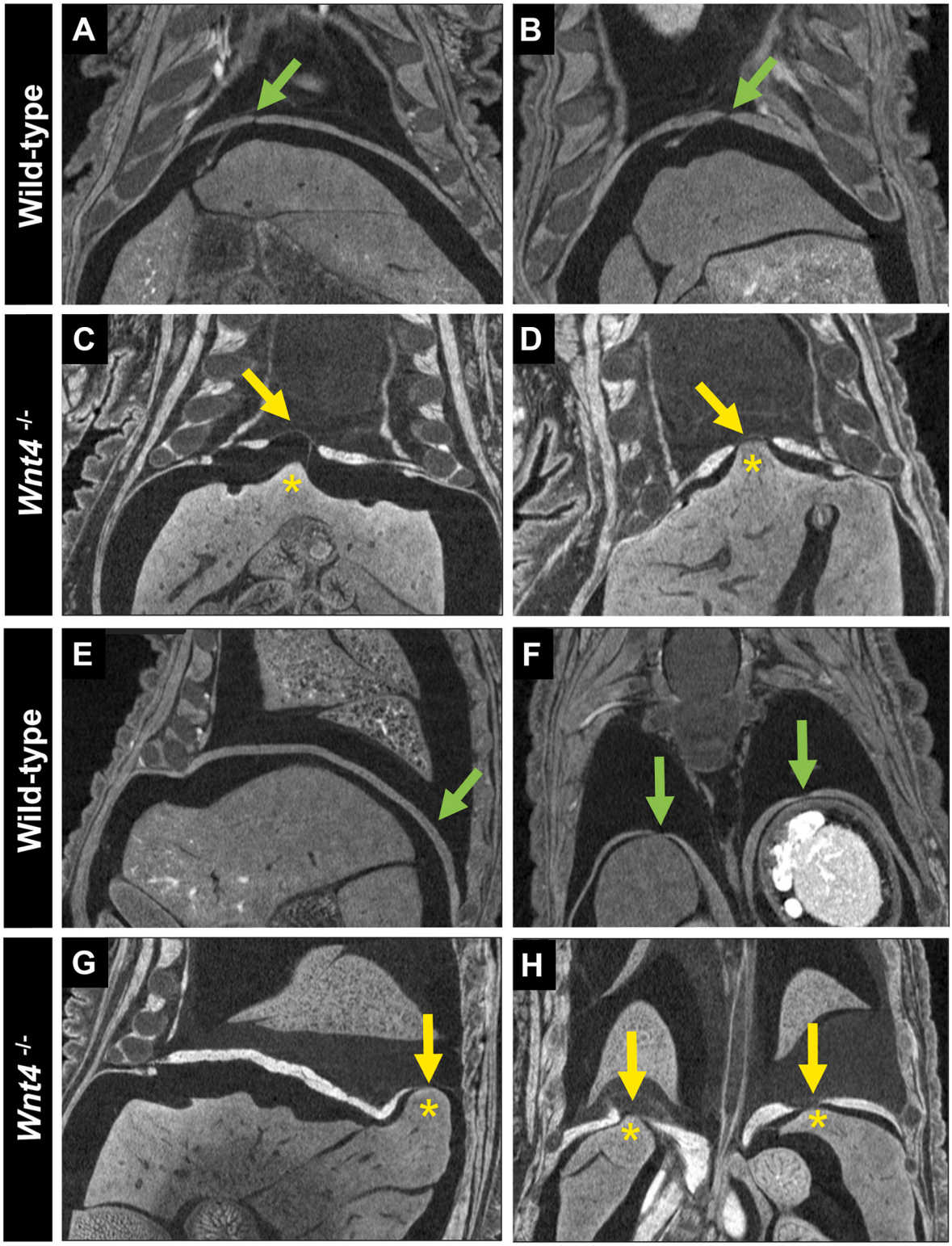

Fig. 8. Micro-CT analyses confirm that *Wnt4*$^{-/-}$ newborn pups have anterior and posterior sac CDH. A, B) Micro-CT analyses (coronal cuts) revealed intact anterior diaphragm musculature in wild-type newborn pups with only a small line of amuscular diaphragm between the right and left muscularized regions (green arrows). C, D) In contrast, *Wnt4*$^{-/-}$ newborn pups have anterior sac CDH as evidenced by domed diaphragmic membranes (yellow arrows) overlying outgrowths of liver (*). E) Micro-CT analyses (sagittal cuts) revealed intact posterior diaphragm musculature in a wild-type neonate (green arrow). F) Micro-CT analyses (coronal cuts) of a second wilt-type neonate revealed intact posterior musculature with only the small line of amuscular diaphragm separating the muscularized region of the right and left hemidiaphragm (green arrows) and no evidence of herniation. G) Micro-CT analyses (sagittal cuts) of a *Wnt4*$^{-/-}$ neonate revealed herniated liver tissue (*) covered by a membranous sac (yellow arrow). H) Micro-CT analyses (coronal cuts) of a second *Wnt4*$^{-/-}$ newborn pup revealed bilateral sac CDH as evidenced by regions of herniated liver tissue (*) covered by membranous sacs (yellow arrows).

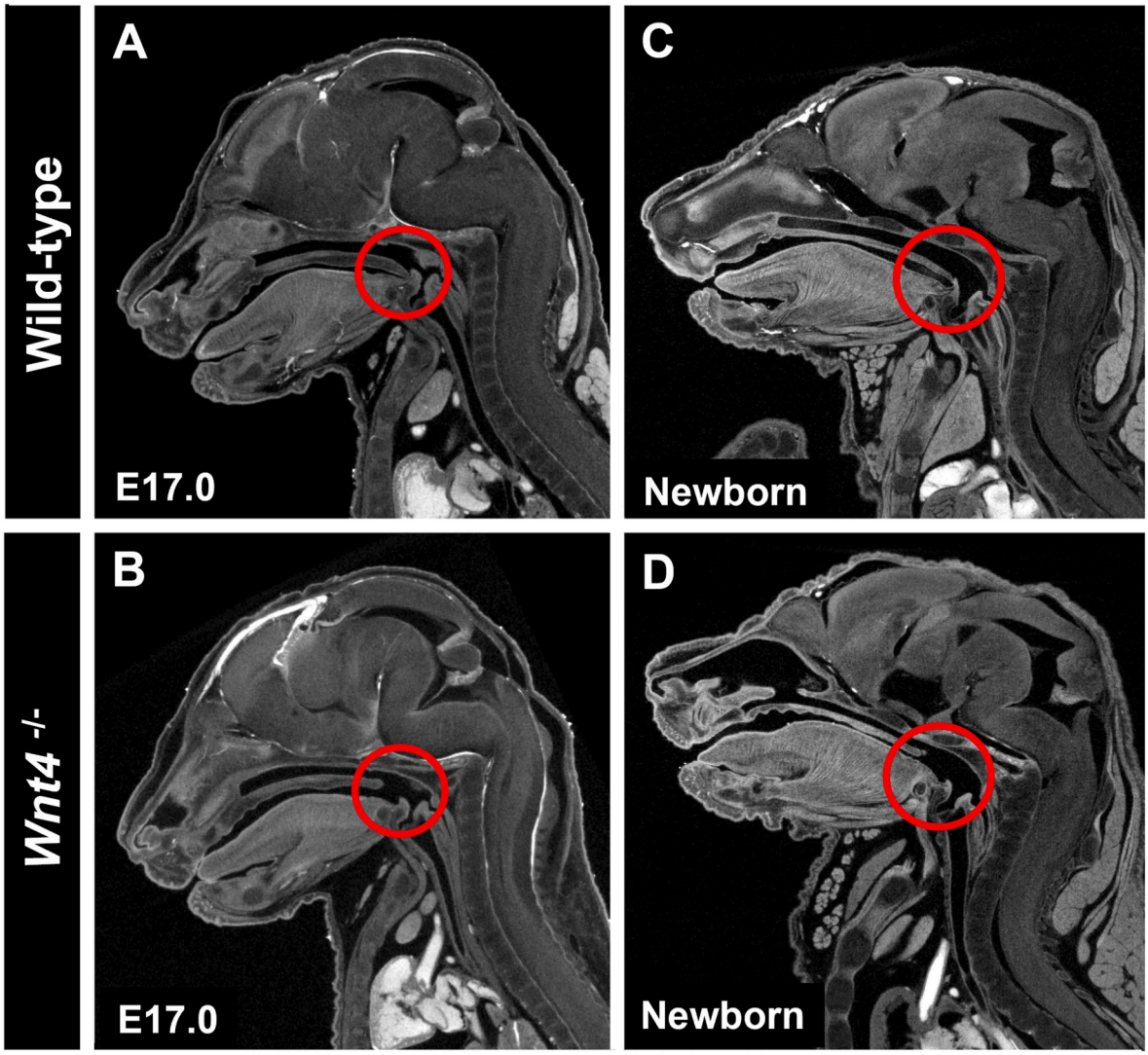

Fig. 9. *Wnt4*$^{-/-}$ embryos and mice have soft palate clefts. A, B) Micro-CT analyses revealed soft palate clefts in *Wnt4*$^{-/-}$ embryos at E17.0 compared to wild-type control littermates (red circles). C, D) A soft palate cleft seen in a *Wnt4*$^{-/-}$ neonate compared to a wild-type littermate control (red circles).

and *Wnt4*$^{+/-}$ littermates (Hernandez-Garcia et al., 2023). They went on to show that *Wnt4*$^{+/-}$ embryos, and to a much greater extent *Sox7*$^{+/-}$; *Wnt4*$^{+/-}$ embryos, had decreased mesenchymal cell density in their AV endocardial cushions compared to wild-type embryos. This suggested that the combination of *Wnt4* and *Sox7* haploinsufficiency caused VSDs through their combined effects on endocardial cushion development (Hernandez-Garcia et al., 2023).

Our identification of VSDs in 44.4% (8/18) of the *Wnt4*$^{-/-}$ embryos and newborn pups analyzed in this study, and a lack of VSDs seen in 0% (0/19) of wild-type controls, provides statistically significant evidence ($P = 0.0011$) that decreased WNT4 function is sufficient to cause VSDs in mammals. These results also suggest that VSD is likely to be an incompletely penetrant phenotype in individuals with SERKAL syndrome.

4.5. *WNT4 loss of function as a cause of diaphragm defects*

Both of the individuals with SERKAL syndrome and CDH had bilateral diaphragm agenesis, a severe form of CDH where all or part of the diaphragm fails to develop. The central tendon of the diaphragm, the diaphragmatic musculature, and the diaphragmatic connective tissue develop from three structures present in the embryo; the septum transversum, the somites, and the pleuroperitoneal folds (PPFs) (Merrell and Kardon, 2013). The septum transversum, a thin, mesodermal sheet of tissue, serves as the original barrier between the abdominal and thoracic cavities and is thought to provide a scaffold for diaphragm morphogenesis. Hence, failure to form the septum transversum could result in bilateral diaphragm agenesis. Alternatively, a generalized failure diaphragm muscularization could leave only a membranous diaphragm that is incapable of restraining the abdominal contents leading to herniation. However, no membranous covering or sac was identified in the SERKAL fetuses with diaphragm agenesis (Fig. 3).

The identification of CDH in *Wnt4*$^{-/-}$ embryos and newborn pups provides additional evidence that WNT4 deficiency can cause diaphragm defects in mammals. As is the case with other CDH genes, the pattern of the diaphragmatic hernias differs between WNT4 deficient humans and mice (Jay et al., 2007; Wat et al., 2012). Specifically, *Wnt4*$^{-/-}$ embryos and new born pups do not have diaphragm agenesis as seen in individuals SERKAL syndrome. Instead, their membranous diaphragms are intact but there are areas with decreased or absent muscularization leading to anterior and posterior sac hernias. This pattern of CDH suggests a primary defect in the PPFs—two transient, pyramidal-shaped structures that are the source of the diaphragm's muscle connective tissue and regulate diaphragm muscle development. Abnormalities of the PPF can lead to defective generation/migration of cell populations and impaired muscularization of the diaphragm (Edel et al., 2021; Merrell et al., 2015).

The molecular mechanism by which WNT4 deficiency causes anterior and posterior sac CDH is unknown. However, depletion of *Wnt4*'s upstream activator, SOX7, can cause diaphragm defects with a subset of $Sox7^{+/-}$ mice developing anterior sac CDH similar to what we have observed in $Wnt4^{-/-}$ mice (Wat et al., 2012). Previous studies have suggested that SOX7 expression in mice is limited to the vascular epithelium of blood vessels surrounding the PPF and within the developing diaphragm (Wat et al., 2012). Based on this expression pattern, it was hypothesized that SOX7 may play a role in normal diaphragm development by regulating the expression of signaling molecules including WNTs (Wat et al., 2012). Additional studies will be needed to test this hypothesis and determine WNT4's downstream targets.

4.6. *WNT4 loss of function as a cause of soft palate clefts in mice*

A variety of WNT signaling genes have been associated with orofacial clefting in human and mice (Reynolds et al., 2019). However, WNT4's role in in palatal development has not been previously recognized. $Wnt4^{-/-}$ embryos do not have CL ± P as seen in humans with SERKAL syndrome. Their palatal defects are limited to soft palate clefts (Fig. 7). Additional studies will be needed to determine the underlying cause of the phenotypic differences between humans and mice and to determine the molecular basis by which WNT4 deficiency causes OFC.

4.7. *Identifying additional phenotypes in previously analyzed mouse models*

In some instances, critical phenotypes may be overlooked during the initial phenotyping of mouse models but can be readily identified in targeted studies (Beck et al., 2013; Jordan et al., 2018; Kim et al., 2021). Female *Wnt4* null mice have previously been shown to have various defects analogous to those seen in humans with Mullerian aplasia hyperandrogenism. These phenotypes include masculinized genitalia, absence of the Mullerian duct, atretic kidneys, reduced oocyte numbers, and failure of Leydig cell development in the ovary leading to ectopically activated testosterone biosynthesis (Stark et al., 1994; Vainio et al., 1999). Although no cardiac, diaphragmatic, or palatal anomalies were previously described in these mice, our targeted studies revealed VSDs, anterior and posterior sac CDH, and soft palate clefts in a subset of $Wnt4^{-/-}$ embryos and new born pups. These discoveries underscore the utility of targeted mouse phenotyping in confirming the roles of genes during mammalian development. It is possible that future studies will identify additional defects in *Wnt4* null embryos and mice, or in *Wnt4* conditional knockout models.

5. Conclusion

Our findings suggest that WNT4 deficiency can cause VSD, CDH, and OFC in mice and humans with SERKAL syndrome. These studies also suggest that our machine learning approach can be used as a candidate gene prioritization tool, and that targeted mouse phenotyping can serve as a means of confirming the roles of genes in mammalian development.

CRediT authorship contribution statement

Andrés Hernández-García: Conceptualization, Formal analysis, Investigation, Visualization, Writing – review & editing. **Bum Jun Kim:** Visualization, Writing – review & editing. **David Chitayat:** Formal analysis, Investigation, Writing – review & editing. **Patrick Shannon:** Formal analysis, Investigation, Visualization, Writing – review & editing. **Stephanie Hedges:** Formal analysis, Investigation, Writing – review & editing. **Maria Al Bandari:** Formal analysis, Investigation, Writing – review & editing. **Maria J. Guillen Sacoto:** Formal analysis, Investigation, Writing – review & editing. **Emily Anne Bates:** Formal analysis, Investigation, Visualization, Writing – review & editing. **Yunus H. Ozekin:** Formal analysis, Investigation, Visualization, Writing – review & editing. **Victor Faundes:** Formal analysis, Investigation, Visualization, Writing – review & editing. **Pamela N. Luna:** Software, Writing – review & editing. **Chad A. Shaw:** Software, Supervision, Writing – review & editing. **Tara L. Rasmussen:** Investigation, Methodology, Writing – review & editing. **Chih-Wei Hsu:** Methodology, Visualization, Writing – review & editing. **Daryl A. Scott:** Conceptualization, Formal analysis, Funding acquisition, Supervision, Visualization, Writing – original draft, Writing – review & editing.

Funding

This work was supported, in part, by a National Institutes of Health grant [R01-HD098458] to D.A.S.

Competing interests

MJGS is an employee of, and may own stock in, GeneDx. The Department of Molecular & Human Genetics at Baylor College of Medicine receives revenue from clinical genetic testing completed at Baylor Genetics. All other authors have no competing interests to declare.

Acknowledgements

Molecular graphics and analyses performed with UCSF ChimeraX, developed by the Resource for Biocomputing, Visualization, and Informatics at the University of California, San Francisco, with support from National Institutes of Health R01-GM129325 and the Office of Cyber Infrastructure and Computational Biology, National Institute of Allergy and Infectious Diseases.

Appendix A. Supplementary data

Supplementary data to this article can be found online at https://doi.org/10.1016/j.ydbio.2025.09.016.

Data availability

Sequence variant information has been submitted to ClinVar (https://submit.ncbi.nlm.nih.gov/clinvar/).

References

Alfieri, C.M., Cheek, J., Chakraborty, S., Yutzey, K.E., 2010. Wnt signaling in heart valve development and osteogenic gene induction. Dev. Biol. 338, 127–135. https://doi.org/10.1016/j.ydbio.2009.11.030.

Ashburner, M., Ball, C.A., Blake, J.A., Botstein, D., Butler, H., Cherry, J.M., Davis, A.P., Dolinski, K., Dwight, S.S., Eppig, J.T., Harris, M.A., Hill, D.P., Issel-Tarver, L., Kasarskis, A., Lewis, S., Matese, J.C., Richardson, J.E., Ringwald, M., Rubin, G.M., Sherlock, G., 2000. Gene ontology: tool for the unification of biology. The Gene Ontology Consortium. Nat. Genet. 25, 25–29. https://doi.org/10.1038/75556.

Babai, A., Irving, M., 2023. Orofacial clefts: genetics of cleft lip and palate. Genes 14. https://doi.org/10.3390/genes14081603.

Beck, T.F., Veenma, D., Shchelochkov, O.A., Yu, Z., Kim, B.J., Zaveri, H.P., van Bever, Y., Choi, S., Douben, H., Bertin, T.K., Patel, P.I., Lee, B., Tibboel, D., de Klein, A., Stockton, D.W., Justice, M.J., Scott, D.A., 2013. Deficiency of FRAS1-related extracellular matrix 1 (FREM1) causes congenital diaphragmatic hernia in humans and mice. Hum. Mol. Genet. 22, 1026–1038. https://doi.org/10.1093/hmg/dds507.

Belanger Deloge, R., Zhao, X., Luna, P.N., Shaw, C.A., Rosenfeld, J.A., Scott, D.A., 2023. High molecular diagnostic yields and novel phenotypic expansions involving syndromic anorectal malformations. Eur. J. Hum. Genet. : EJHG (Eur. J. Hum. Genet.) 31, 296–303. https://doi.org/10.1038/s41431-022-01255-y.

Biason-Lauber, A., Konrad, D., Navratil, F., Schoenle, E.J., 2004. A WNT4 mutation associated with Mullerian-duct regression and virilization in a 46,XX woman. N. Engl. J. Med. 351, 792–798. https://doi.org/10.1056/NEJMoa040533.

Biason-Lauber, A., De Filippo, G., Konrad, D., Scarano, G., Nazzaro, A., Schoenle, E.J., 2007. WNT4 deficiency–a clinical phenotype distinct from the classic Mayer-Rokitansky-Kuster-Hauser syndrome: a case report. Hum. Reprod. 22, 224–229. https://doi.org/10.1093/humrep/del360.

Blake, J.A., Bult, C.J., Eppig, J.T., Kadin, J.A., Richardson, J.E., Mouse Genome Database, G., 2014. The Mouse Genome Database: integration of and access to knowledge about the laboratory mouse. Nucleic Acids Res. 42, D810–D817. https://doi.org/10.1093/nar/gkt1225.

Brown, J.M., Horner, N.R., Lawson, T.N., Fiegel, T., Greenaway, S., Morgan, H., Ring, N., Santos, L., Sneddon, D., Teboul, L., Vibert, J., Yaikhom, G., Westerberg, H., Mallon, A.-M., 2016. A bioimage informatics platform for high-throughput embryo phenotyping. Briefings Bioinf. 19, 41–51. https://doi.org/10.1093/bib/bbw101.

Callaway, D.A., Campbell, I.M., Stover, S.R., Hernandez-Garcia, A., Jhangiani, S.N., Punetha, J., Paine, I.S., Posey, J.E., Muzny, D., Lally, K.P., Lupski, J.R., Shaw, C.A., Fernandes, C.J., Scott, D.A., 2018. Prioritization of candidate genes for congenital diaphragmatic hernia in a critical region on chromosome 4p16 using a machine-learning algorithm. J. Pediatr. Genet. 7, 164–173. https://doi.org/10.1055/s-0038-1655755.

Campbell, I.M., Rao, M., Arredondo, S.D., Lalani, S.R., Xia, Z., Kang, S.H., Bi, W., Breman, A.M., Smith, J.L., Bacino, C.A., Beaudet, A.L., Patel, A., Cheung, S.W., Lupski, J.R., Stankiewicz, P., Ramocki, M.B., Shaw, C.A., 2013. Fusion of large-scale genomic knowledge and frequency data computationally prioritizes variants in epilepsy. PLoS Genet. 9, e1003797. https://doi.org/10.1371/journal.pgen.1003797.

Cervantes-Salazar, J.L., Perez-Hernandez, N., Calderon-Colmenero, J., Rodriguez-Perez, J.M., Gonzalez-Pacheco, M.G., Villamil-Castaneda, C., Rosas-Tlaque, A.A., Ortega-Zhindon, D.B., 2024. Genetic insights into congenital cardiac septal defects-A narrative review. Biology 13. https://doi.org/10.3390/biology13110911.

Chaithra, S., Agarwala, S., Ramachandra, N.B., 2022. High-risk genes involved in common septal defects of congenital heart disease. Gene 840, 146745. https://doi.org/10.1016/j.gene.2022.146745.

Combs, M.D., Yutzey, K.E., 2009. Heart valve development: regulatory networks in development and disease. Circ. Res. 105, 408–421. https://doi.org/10.1161/CIRCRESAHA.109.201566.

Cowley, M.J., Pinese, M., Kassahn, K.S., Waddell, N., Pearson, J.V., Grimmond, S.M., Biankin, A.V., Hautaniemi, S., Wu, J., 2012. PINA v2.0: mining interactome modules. Nucleic Acids Res. 40, D862–D865. https://doi.org/10.1093/nar/gkr967.

Edel, G.G., Schaaf, G., Wijnen, R.M.H., Tibboel, D., Kardon, G., Rottier, R.J., 2021. Cellular origin(s) of congenital diaphragmatic hernia. Front Pediatr 9, 804496. https://doi.org/10.3389/fped.2021.804496.

Eisenberg, L.M., Markwald, R.R., 1995. Molecular regulation of atrioventricular valvuloseptal morphogenesis. Circ. Res. 77, 1–6.

Fedorov, A., Beichel, R., Kalpathy-Cramer, J., Finet, J., Fillion-Robin, J.C., Pujol, S., Bauer, C., Jennings, D., Fennessy, F., Sonka, M., Buatti, J., Aylward, S., Miller, J.V., Pieper, S., Kikinis, R., 2012. 3D Slicer as an image computing platform for the quantitative imaging network. Magn. Reson. Imaging 30, 1323–1341. https://doi.org/10.1016/j.mri.2012.05.001.

Hardcastle, A., Berry, A.M., Campbell, I.M., Zhao, X., Liu, P., Gerard, A.E., Rosenfeld, J. A., Sisoudiya, S.D., Hernandez-Garcia, A., Loddo, S., Di Tommaso, S., Novelli, A., Dentici, M.L., Capolino, R., Digilio, M.C., Graziani, L., Rustad, C.F., Neas, K., Ferrero, G.B., Brusco, A., Di Gregorio, E., Wellesley, D., Beneteau, C., Joubert, M., Van Den Bogaert, K., Boogaerts, A., McMullan, D.J., Dean, J., Giuffrida, M.G., Bernardini, L., Varghese, V., Shannon, N.L., Harrison, R.E., Lam, W.W.K., McKee, S., Turnpenny, P.D., Cole, T., Morton, J., Eason, J., Jones, M.C., Hall, R., Wright, M., Horridge, K., Shaw, C.A., Chung, W.K., Scott, D.A., 2022. Identifying phenotypic expansions for congenital diaphragmatic hernia plus (CDH+) using DECIPHER data. Am. J. Med. Genet. 188, 2958–2968. https://doi.org/10.1002/ajmg.a.62919.

Hernandez-Garcia, A., Pendleton, K.E., Kim, S., Li, Y., Kim, B.J., Zaveri, H.P., Jordan, V. K., Berry, A.M., Ljungberg, M.C., Chen, R., Lanz, R.B., Scott, D.A., 2023. SOX7 deficiency causes ventricular septal defects through its effects on endocardial-to-mesenchymal transition and the expression of Wnt4 and Bmp2. Hum. Mol. Genet. 32, 2152–2161. https://doi.org/10.1093/hmg/ddad050.

Hong, N., Zhang, E., Xie, H., Jin, L., Zhang, Q., Lu, Y., Chen, A.F., Yu, Y., Zhou, B., Chen, S., Yu, Y., Sun, K., 2021. The transcription factor Sox7 modulates endocardiac cushion formation contributed to atrioventricular septal defect through Wnt4/Bmp2 signaling. Cell Death Dis. 12, 393. https://doi.org/10.1038/s41419-021-03658-z.

Hsu, C.W., Kalaga, S., Akoma, U., Rasmussen, T.L., Christiansen, A.E., Dickinson, M.E., 2019. High resolution imaging of mouse embryos and neonates with X-Ray micro-computed tomography. Curr Protoc Mouse Biol 9, e63. https://doi.org/10.1002/cpmo.63.

Huth, E.A., Zhao, X., Owen, N., Luna, P.N., Vogel, I., Dorf, I.L.H., Joss, S., Clayton-Smith, J., Parker, M.J., Louw, J.J., Gewillig, M., Breckpot, J., Kraus, A., Sasaki, E., Kini, U., Burgess, T., Tan, T.Y., Armstrong, R., Neas, K., Ferrero, G.B., Brusco, A., Kerstjens-Frederikse, W.S., Rankin, J., Helvaty, L.R., Landis, B.J., Geddes, G.C., McBride, K.L., Ware, S.M., Shaw, C.A., Lalani, S.R., Rosenfeld, J.A., Scott, D.A., 2023. Clinical exome sequencing efficacy and phenotypic expansions involving anomalous pulmonary venous return. Eur. J. Hum. Genet. : EJHG (Eur. J. Hum. Genet.) 31, 1430–1439. https://doi.org/10.1038/s41431-023-01451-4.

Ioannidis, N.M., Rothstein, J.H., Pejaver, V., Middha, S., McDonnell, S.K., Baheti, S., Musolf, A., Li, Q., Holzinger, E., Karyadi, D., Cannon-Albright, L.A., Teerlink, C.C., Stanford, J.L., Isaacs, W.B., Xu, J., Cooney, K.A., Lange, E.M., Schleutker, J., Carpten, J.D., Powell, I.J., Cussenot, O., Cancel-Tassin, G., Giles, G.G., MacInnis, R. J., Maier, C., Hsieh, C.L., Wiklund, F., Catalona, W.J., Foulkes, W.D., Mandal, D., Eeles, R.A., Kote-Jarai, Z., Bustamante, C.D., Schaid, D.J., Hastie, T., Ostrander, E.A., Bailey-Wilson, J.E., Radivojac, P., Thibodeau, S.N., Whittemore, A.S., Sieh, W., 2016. REVEL: an Ensemble method for predicting the Pathogenicity of rare missense variants. Am. J. Hum. Genet. 99, 877–885. https://doi.org/10.1016/j.ajhg.2016.08.016.

Janda, C.Y., Waghray, D., Levin, A.M., Thomas, C., Garcia, K.C., 2012. Structural basis of wnt recognition by frizzled. Science 337, 59–64. https://doi.org/10.1126/science.1222879.

Jay, P.Y., Bielinska, M., Erlich, J.M., Mannisto, S., Pu, W.T., Heikinheimo, M., Wilson, D. B., 2007. Impaired mesenchymal cell function in Gata4 mutant mice leads to diaphragmatic hernias and primary lung defects. Dev. Biol. 301, 602–614. https://doi.org/10.1016/j.ydbio.2006.09.050.

Jordan, V.K., Beck, T.F., Hernandez-Garcia, A., Kundert, P.N., Kim, B.J., Jhangiani, S.N., Gambin, T., Starkovich, M., Punetha, J., Paine, I.S., Posey, J.E., Li, A.H., Muzny, D., Hsu, C.W., Lashua, A.J., Sun, X., Fernandes, C.J., Dickinson, M.E., Lally, K.P., Gibbs, R.A., Boerwinkle, E., Lupski, J.R., Scott, D.A., 2018. The role of FREM2 and FRAS1 in the development of congenital diaphragmatic hernia. Hum. Mol. Genet. 27, 2064–2075. https://doi.org/10.1093/hmg/ddy110.

Kanehisa, M., Goto, S., Furumichi, M., Tanabe, M., Hirakawa, M., 2010. KEGG for representation and analysis of molecular networks involving diseases and drugs. Nucleic Acids Res. 38, D355–D360. https://doi.org/10.1093/nar/gkp896.

Kaneko, K., Li, X., Zhang, X., Lamberti, J.J., Jamieson, S.W., Thistlethwaite, P.A., 2008. Endothelial expression of bone morphogenetic protein receptor type 1a is required for atrioventricular valve formation. Ann. Thorac. Surg. 85, 2090–2098. https://doi.org/10.1016/j.athoracsur.2008.02.027.

Karczewski, K.J., Francioli, L.C., Tiao, G., Cummings, B.B., Alfoldi, J., Wang, Q., Collins, R.L., Laricchia, K.M., Ganna, A., Birnbaum, D.P., Gauthier, L.D., Brand, H., Solomonson, M., Watts, N.A., Rhodes, D., Singer-Berk, M., England, E.M., Seaby, E. G., Kosmicki, J.A., Walters, R.K., Tashman, K., Farjoun, Y., Banks, E., Poterba, T., Wang, A., Seed, C., Whiffin, N., Chong, J.X., Samocha, K.E., Pierce-Hoffman, E., Zappala, Z., O'Donnell-Luria, A.H., Minikel, E.V., Weisburd, B., Lek, M., Ware, J.S., Vittal, C., Armean, I.M., Bergelson, L., Cibulskis, K., Connolly, K.M., Covarrubias, M., Donnelly, S., Ferriera, S., Gabriel, S., Gentry, J., Gupta, N., Jeandet, T., Kaplan, D., Llanwarne, C., Munshi, R., Novod, S., Petrillo, N., Roazen, D., Ruano-Rubio, V., Saltzman, A., Schleicher, M., Soto, J., Tibbetts, K., Tolonen, C., Wade, G., Talkowski, M.E., Genome Aggregation Database, C., Neale, B.M., Daly, M.J., MacArthur, D.G., 2020. The mutational constraint spectrum quantified from variation in 141,456 humans. Nature 581, 434–443. https://doi.org/10.1038/s41586-020-2308-7.

Katoh, K., Misawa, K., Kuma, K., Miyata, T., 2002. MAFFT: a novel method for rapid multiple sequence alignment based on fast Fourier transform. Nucleic Acids Res. 30, 3059–3066. https://doi.org/10.1093/nar/gkf436.

Khan, M.I., Cs, P., Srinath, N.M., 2020. Genetic factors in nonsyndromic orofacial clefts. Glob Med Genet 7, 101–108. https://doi.org/10.1055/s-0041-1722951.

Kim, B.J., Zaveri, H.P., Kundert, P.N., Jordan, V.K., Scott, T.M., Carmichael, J., Scott, D. A., 2021. RERE deficiency contributes to the development of orofacial clefts in humans and mice. Hum. Mol. Genet. 30, 595–602. https://doi.org/10.1093/hmg/ddab084.

Kobayashi, A., Valerius, M.T., Mugford, J.W., Carroll, T.J., Self, M., Oliver, G., McMahon, A.P., 2008. Six2 defines and regulates a multipotent self-renewing nephron progenitor population throughout mammalian kidney development. Cell Stem Cell 3, 169–181. https://doi.org/10.1016/j.stem.2008.05.020.

Kovacic, J.C., Dimmeler, S., Harvey, R.P., Finkel, T., Aikawa, E., Krenning, G., Baker, A. H., 2019. Endothelial to mesenchymal transition in cardiovascular disease: JACC state-of-the-art review. J. Am. Coll. Cardiol. 73, 190–209. https://doi.org/10.1016/j.jacc.2018.09.089.

Kunisetty, B., Martin-Giacalone, B.A., Zhao, X., Luna, P.N., Brooks, B.P., Hufnagel, R.B., Shaw, C.A., Rosenfeld, J.A., Agopian, A.J., Lupo, P.J., Scott, D.A., 2024. High clinical exome sequencing diagnostic rates and novel phenotypic expansions for nonisolated microphthalmia, anophthalmia, and coloboma. Investigative ophthalmology & visual science 65, 25. https://doi.org/10.1167/iovs.65.3.25.

Leslie, E.J., Marazita, M.L., 2013. Genetics of cleft lip and cleft palate. Am. J. Med. Genet. Part C, Seminars in medical genetics 163C, 246–258. https://doi.org/10.1002/ajmg.c.31381.

Lin, C.J., Lin, C.Y., Chen, C.H., Zhou, B., Chang, C.P., 2012. Partitioning the heart: mechanisms of cardiac septation and valve development. Development 139, 3277–3299. https://doi.org/10.1242/dev.063495.

Ma, L., Lu, M.F., Schwartz, R.J., Martin, J.F., 2005. Bmp2 is essential for cardiac cushion epithelial-mesenchymal transition and myocardial patterning. Development 132, 5601–5611. https://doi.org/10.1242/dev.02156.

Mandel, H., Shemer, R., Borochowitz, Z.U., Okopnik, M., Knopf, C., Indelman, M., Drugan, A., Tiosano, D., Gershoni-Baruch, R., Choder, M., Sprecher, E., 2008. SERKAL syndrome: an autosomal-recessive disorder caused by a loss-of-function mutation in WNT4. Am. J. Hum. Genet. 82, 39–47. https://doi.org/10.1016/j.ajhg.2007.08.005.

Meng, E.C., Goddard, T.D., Pettersen, E.F., Couch, G.S., Pearson, Z.J., Morris, J.H., Ferrin, T.E., 2023. UCSF ChimeraX: tools for structure building and analysis. Protein Sci. 32, e4792. https://doi.org/10.1002/pro.4792.

Merrell, A.J., Kardon, G., 2013. Development of the diaphragm – a skeletal muscle essential for mammalian respiration. FEBS J. 280, 4026–4035. https://doi.org/10.1111/febs.12274.

Merrell, A.J., Ellis, B.J., Fox, Z.D., Lawson, J.A., Weiss, J.A., Kardon, G., 2015. Muscle connective tissue controls development of the diaphragm and is a source of congenital diaphragmatic hernias. Nat. Genet. 47, 496–504. https://doi.org/10.1038/ng.3250.

Mossey, P.A., Modell, B., 2012. Epidemiology of oral clefts 2012: an international perspective. Front Oral Biol 16, 1–18. https://doi.org/10.1159/000337464.

Nusse, R., Clevers, H., 2017. Wnt/beta-Catenin signaling, disease, and emerging therapeutic modalities. Cell 169, 985–999. https://doi.org/10.1016/j.cell.2017.05.016.

olitis, M.D., Bermejo-Sanchez, E., Canfield, M.A., Contiero, P., Cragan, J.D., Dastgiri, S., de Walle, H.E.K., Feldkamp, M.L., Nance, A., Groisman, B., Gatt, M., Benavides-Lara, A., Hurtado-Villa, P., Kallen, K., Landau, D., Lelong, N., Lopez-Camelo, J., Martinez, L., Morgan, M., Mutchinick, O.M., Pierini, A., Rissmann, A., Sipek, A., Szabova, E., Wertelecki, W., Zarante, I., Bakker, M.K., Kancherla, V., Mastroiacovo, P., Nembhard, W.N., 2021. International Clearinghouse for Birth Defects, S. & Research. Prevalence and mortality in children with congenital

diaphragmatic hernia: a multicountry study. Ann. Epidemiol. 56, 61–69 e63. https://doi.org/10.1016/j.annepidem.2020.11.007.
Ozekin, Y.H., O'Rourke, R., Bates, E.A., 2023. Single cell sequencing of the mouse anterior palate reveals mesenchymal heterogeneity. Dev. Dyn. : an official publication of the American Association of Anatomists 252, 713–727. https://doi.org/10.1002/dvdy.573.
Perrot, A., Rickert-Sperling, S., 2024. Human genetics of ventricular septal defect. Advances in experimental medicine and biology 1441, 505–534. https://doi.org/10.1007/978-3-031-44087-8_27.
Pettersen, E.F., Goddard, T.D., Huang, C.C., Couch, G.S., Greenblatt, D.M., Meng, E.C., Ferrin, T.E., 2004. UCSF Chimera–a visualization system for exploratory research and analysis. J. Comput. Chem. 25, 1605–1612. https://doi.org/10.1002/jcc.20084.
Philibert, P., Biason-Lauber, A., Rouzier, R., Pienkowski, C., Paris, F., Konrad, D., Schoenle, E., Sultan, C., 2008. Identification and functional analysis of a new WNT4 gene mutation among 28 adolescent girls with primary amenorrhea and mullerian duct abnormalities: a French collaborative study. The Journal of clinical endocrinology and metabolism 93, 895–900. https://doi.org/10.1210/jc.2007-2023.
Qiao, L., Xu, L., Yu, L., Wynn, J., Hernan, R., Zhou, X., Farkouh-Karoleski, C., Krishnan, U.S., Khlevner, J., De, A., Zygmunt, A., Crombleholme, T., Lim, F.Y., Needelman, H., Cusick, R.A., Mychaliska, G.B., Warner, B.W., Wagner, A.J., Danko, M.E., Chung, D., Potoka, D., Kosinski, P., McCulley, D.J., Elfiky, M., Azarow, K., Fialkowski, E., Schindel, D., Soffer, S.Z., Lyon, J.B., Zalieckas, J.M., Vardarajan, B.N., Aspelund, G., Duron, V.P., High, F.A., Sun, X., Donahoe, P.K., Shen, Y., Chung, W.K., 2021. Rare and de novo variants in 827 congenital diaphragmatic hernia probands implicate LONP1 as candidate risk gene. Am. J. Hum. Genet. 108, 1964–1980. https://doi.org/10.1016/j.ajhg.2021.08.011.
Retterer, K., Juusola, J., Cho, M.T., Vitazka, P., Millan, F., Gibellini, F., Vertino-Bell, A., Smaoui, N., Neidich, J., Monaghan, K.G., McKnight, D., Bai, R., Suchy, S., Friedman, B., Tahiliani, J., Pineda-Alvarez, D., Richard, G., Brandt, T., Haverfield, E., Chung, W.K., Bale, S., 2016. Clinical application of whole-exome sequencing across clinical indications. Genet. Med. : official journal of the American College of Medical Genetics 18, 696–704. https://doi.org/10.1038/gim.2015.148.
Reynolds, K., Kumari, P., Sepulveda Rincon, L., Gu, R., Ji, Y., Kumar, S., Zhou, C.J., 2019. Wnt signaling in orofacial clefts: crosstalk, pathogenesis and models. Dis. Model. Mech. 12. https://doi.org/10.1242/dmm.037051.
Rivera-Feliciano, J., Tabin, C.J., 2006. Bmp2 instructs cardiac progenitors to form the heart-valve-inducing field. Dev. Biol. 295, 580–588. https://doi.org/10.1016/j.ydbio.2006.03.043.
Russell, M.K., Longoni, M., Wells, J., Maalouf, F.I., Tracy, A.A., Loscertales, M., Ackerman, K.G., Pober, B.R., Lage, K., Bult, C.J., Donahoe, P.K., 2012. Congenital diaphragmatic hernia candidate genes derived from embryonic transcriptomes. Proceedings of the National Academy of Sciences of the United States of America 109, 2978–2983. https://doi.org/10.1073/pnas.1121621109.
Schubach, M., Maass, T., Nazaretyan, L., Roner, S., Kircher, M., 2024. CADD v1.7: using protein language models, regulatory CNNs and other nucleotide-level scores to improve genome-wide variant predictions. Nucleic Acids Res. 52, D1143–D1154. https://doi.org/10.1093/nar/gkad989.
Schwarz, J.M., Cooper, D.N., Schuelke, M., Seelow, D., 2014. MutationTaster2: mutation prediction for the deep-sequencing age. Nat. Methods 11, 361–362. https://doi.org/10.1038/nmeth.2890.
Scott, T.M., Campbell, I.M., Hernandez-Garcia, A., Lalani, S.R., Liu, P., Shaw, C.A., Rosenfeld, J.A., Scott, D.A., 2021. Clinical exome sequencing data reveal high diagnostic yields for congenital diaphragmatic hernia plus (CDH+) and new phenotypic expansions involving CDH. J. Med. Genet. 59, 270–278. https://doi.org/10.1136/jmedgenet-2020-107317.
Stark, K., Vainio, S., Vassileva, G., McMahon, A.P., 1994. Epithelial transformation of metanephric mesenchyme in the developing kidney regulated by Wnt-4. Nature 372, 679–683. https://doi.org/10.1038/372679a0.
Stollar, E.J., Smith, D.P., 2020. Uncovering protein structure. Essays Biochem. 64, 649–680. https://doi.org/10.1042/EBC20190042.
Stuart, T., Butler, A., Hoffman, P., Hafemeister, C., Papalexi, E., Mauck 3rd, W.M., Hao, Y., Stoeckius, M., Smibert, P., Satija, R., 2019. Comprehensive integration of single-cell data. Cell 177, e1821. https://doi.org/10.1016/j.cell.2019.05.031, 1888-1902.
Sy, M.R., Chauhan, J., Prescott, K., Imam, A., Kraus, A., Beleza, A., Salkeld, L., Hosdurga, S., Parker, M., Vasudevan, P., Islam, L., Goel, H., Bain, N., Park, S.M., Mohammed, S., Dieterich, K., Coutton, C., Satre, V., Vieville, G., Donaldson, A., Beneteau, C., Ghoumid, J., Van Den Bogaert, K., Boogaerts, A., Boudry, E., Vanlerberghe, C., Petit, F., Bernardini, L., Torres, B., Mattina, T., Carli, D., Mandrile, G., Pinelli, M., Brunetti-Pierri, N., Neas, K., Beddow, R., Torring, P.M., Faletra, F., Spedicati, B., Gasparini, P., Mussa, A., Ferrero, G.B., Lampe, A., Lam, W., Bi, W., Bacino, C.A., Kuwahara, A., Bush, J.O., Zhao, X., Luna, P.N., Shaw, C.A., Rosenfeld, J.A., Scott, D.A., 2022. Exome sequencing efficacy and phenotypic expansions involving esophageal atresia/tracheoesophageal fistula plus. Am. J. Med. Genet. 188, 3492–3504. https://doi.org/10.1002/ajmg.a.62976.
Vainio, S., Heikkila, M., Kispert, A., Chin, N., McMahon, A.P., 1999. Female development in mammals is regulated by Wnt-4 signalling. Nature 397, 405–409. https://doi.org/10.1038/17068.
Wang, Y., Wu, B., Chamberlain, A.A., Lui, W., Koirala, P., Susztak, K., Klein, D., Taylor, V., Zhou, B., 2013. Endocardial to myocardial notch-wnt-bmp axis regulates early heart valve development. PLoS One 8, e60244. https://doi.org/10.1371/journal.pone.0060244.
Wang, J., Al-Ouran, R., Hu, Y., Kim, S.Y., Wan, Y.W., Wangler, M.F., Yamamoto, S., Chao, H.T., Comjean, A., Mohr, S.E., , Udn, Perrimon, N., Liu, Z., Bellen, H.J., 2017. MARRVEL: integration of human and model organism genetic resources to facilitate functional annotation of the human genome. Am. J. Hum. Genet. 100, 843–853. https://doi.org/10.1016/j.ajhg.2017.04.010.
Wat, M.J., Beck, T.F., Hernandez-Garcia, A., Yu, Z., Veenma, D., Garcia, M., Holder, A. M., Wat, J.J., Chen, Y., Mohila, C.A., Lally, K.P., Dickinson, M., Tibboel, D., de Klein, A., Lee, B., Scott, D.A., 2012. Mouse model reveals the role of SOX7 in the development of congenital diaphragmatic hernia associated with recurrent deletions of 8p23.1. Hum. Mol. Genet. 21, 4115–4125. https://doi.org/10.1093/hmg/dds241.
Zhang, Q., Pan, Y., Ji, J., Xu, Y., Zhang, Q., Qin, L., 2021. Roles and action mechanisms of WNT4 in cell differentiation and human diseases: a review. Cell Death Discov. 7, 287. https://doi.org/10.1038/s41420-021-00668-w.